Table 4
The genes used in PART-BFCS class predictor for one set of CNS tumor data set

Accession number	Gene name	Descriptions	Times of selection	Average intensity of surviving patients[a]	Average intensity of dead patients[b]	Threshold of model[c]	Prognostic markers
U20657	USP4	Ubiquitin specific protease 4 (proto-oncogene)	9	796	127	391	[d]
X59798	CCND1	Cyclin D1 (PRAD1: parathyroid adenomatosis 1)	6	0	2176	330	[e]
M73547	C5orf18	Chromosome 5 open reading frame 18	6	1439	275	797	
AB000460	C4orf8	Chromosome 4 open reading frame 8	4	2429	1094	1605	
L33243	PKD1	Polycystic kidney disease 1 (autosomal dominant)	4	1498	228	815	
X13967	LIF	Leukemia inhibitory factor (cholinergic differentiation factor)	2	464	5	206	[f]
L10333	RTN1	Reticulon 1	2	4483	821	1747	
D30756	M17S2	Membrane component, chromosome 17, surface marker 2	1	591	59	236	
D83018	NELL2	NEL-like 2 (chicken)	1	2710	851	1416	
HG2238-HT2321	NUMA1	Nuclear mitotic apparatus protein 1, alt. splice form 2	1	2833	1197	1721	
J04046	CALM3	Calmodulin 3 (phosphorylase kinase, delta)	1	3287	1022	1753	
S76475	NTRK3	Neurotrophic tyrosine kinase, receptor, type 3 (TrkC)	1	2002	96	687	
U25849	ACP1	Acid phosphatase 1, soluble	1	206	1082	602	
Y09616	CES2	Carboxylesterase 2 (intestine, liver)	1	2894	1065	1706	

[a] The average intensity of gene expression in the patients predicted as survivors.
[b] The average intensity of gene expression in the patients predicted as dead.
[c] The threshold of gene expression in the weak learner model.
[d] The marker gene reported by Frederick et al. [23] as a low-risk marker.
[e] The marker gene reported by Tan et al. [20] as a high-risk marker.
[f] The marker gene reported by Park et al. [22] as a low-risk marker.

very useful to select input combination that shows high accuracy by combining low accuracy inputs. But, the application of PIM to high dimensional data, such as microarray data, may cause overfitting. On the other hand, the boosting used in the BFCS is the method that can construct high-accuracy predictor by combining one-gene predictors. Thus, low-accuracy one-gene predictors are hardly selected. It may be for this reason that BFCS showed high performance.

Next, BFCS were compared with PART-BFCS. Average of gene expression for the 40 genes in 10 combinations of four-input models, was calculated for each class (survivors or dead). And average standard deviation (S.D.) of lower gene expression class for 40 genes is shown in Table 6. Table 6 shows that the S.D. of PART-BFCS was lower than one of BFCS. The values of S.D.s were 0.57 for BFCS and 0.39 for PART-BFCS. This tendency is corresponding to the fact previously reported by us [5]. The genes with low S.D. in lower class may show high generalization performance.

3.5. IF-THEN rules extracted from PART-BFCS model

After modeling, the IF-THEN rules for CNS prognosis were obtained from the model of highest blind accuracy among the 10 combinations. The model includes the *CCND1* gene and *USP4* (*UNPH*) gene as known prognostic markers. The IF-THEN rules have been obtained as a matrix that is classified based on expression level of such selected genes (Fig. 4). Using this matrix, simple and precise rules were obtained as follows. The simplest rule is that patients with high expression of *CCND1* gene are likely to exhibit poor prognosis. Six patients showed high expression of *CCND1* gene and five of them were actually dead patients, which corresponds to 28% (5/18) of all the dead

Table 5
Average modeling accuracy of one-input models between BFCS and FNN-SWEEP (%)

	Order of selection		
	Second	Third	Fourth
BFCS	83.3	77.3	79.0
FNN-SWEEP	72.0	68.7	65.7

In this experiment, 10 combinations of four-input models were constructed. Three genes from second to fourth in four-input were selected as combination of genes for each method. The modeling accuracies when these three genes were used alone as one-gene predictors, were calculated for 10 combinations.

Table 6
Average S.D. of gene expression in lower class between BFCS and PART-BFCS

Methods	The S.D.s of lower class
BFCS	0.56
PART-BFCS	0.39

Average of gene expression for the 40 genes in 10 combinations of four-input models were calculated for each class (survivors or dead). And then, average standard deviation (S.D.) of lower gene expression class for 40 genes was calculated.

				CCND1			
				Low		High	
				PKD1			
				Low	High	Low	High
USP4 (UNPH)	Low	*C5orf18*	Low	**3(M), 4(B), 7(M), 8(M), 9(B), 10(M), 12(M), 13(M), 17(M)**	**11(B), 16(M)**	**6(B), 18(M)**	**5(M)**
			High	**2(B)**, *42(B), 55(B)*	*38(M), 44(M), 47(M), 50(M), 57(B)*		
	High		Low	*19(M)*	*40(M), 49(M)*	**1(M)**	**15(M)**
			High	*51(B), 54(M)*	**14(B)** *20(M), 21(M), 37(B), 39(M), 41(M), 43(M), 45(M), 46(B), 48(B), 52(M), 53(B), 58(M), 59(M)*		*56(M)*

Fig. 4. IF-THEN rules in the top two model of PART-BFCS. Since the expression level of each gene can be divided into either high or low groups using fuzzy logic, this model comprised 16 ($=2^4$) fuzzy rules. Numbers in each matrix are identical to the patient numbers previously described by Pomeroy et al. [7]. Numbers in bold type and italic type indicate the poor and good prognosis patients, respectively. Patient numbers are placed in the matrix according to the expression levels of each patient. Patient numbers in the circle represent incorrect classification by the PART-BFCS. (B) indicates sample in blinded data set. (M) indicates sample in modeling data set.

patients. Next simple rule is that patients with low expression of *CCND1* gene and low expression of *USP4* (*UNPH*) gene are likely to exhibit poor prognosis. Nineteen patients showed low expression of *USP4* (*UNPH*) gene and 12 of them were actually dead patients, which corresponds to 92% (12/13) of dead patients showing low expression of the *CCND1* gene. Nineteen patients showed high expression of *USP4* (*UNPH*) gene and low expression of *CCND1* gene, and 18 of them (95%) were actually surviving patients, which corresponds to 69% (18/26) of all the surviving patients. It was found that surviving or dead patients were clustered at specific parts of the matrix. The following rule was also found: patients were likely to exhibit a poor prognosis when the *USP4* (*UNPH*) expression was low and *C5orf18* expression was low. It was also found that on this matrix, two patients showing poor prognosis were incorrectly predicted as showing good prognosis. This may be due to the inability for complete removal of their tumors by CNS surgery.

4. Conclusions

In the present study, we investigated combinations of various filter and wrapper approaches, and found that combination method of PART and BFCS (a kind of boosting) is significantly superior to other methods with regard to high prediction accuracy for construction of class predictor from gene expression data. This method could select some marker genes related to cancer outcome. In addition, we proposed improved RI_{BFCS} of PART-BFCS. Based on this new index, the discriminated group with over 90% prediction accuracy was separated from the others. It is necessary that there are about 90% or more prediction accuracy in the practical diagnosis application. These results suggest that the PART-BFCS method has a high potential to function as a new method of marker gene selection for the diagnosis of patients, using high dimensional data such as DNA microarray, mass spectrometry (MS), and two-dimensional polyacrylamide gel electrophoresis (2D-PAGE).

Acknowledgment

This work was supported by the Hori Information Science Promotion Foundation for financial support.

References

[1] T. Ando, M. Suguro, T. Hanai, T. Kobayashi, H. Honda, M. Seto, Fuzzy neural network applied to gene expression profiling for predicting the prognosis of diffuse large B-cell lymphoma, Jpn. J. Cancer Res. 93 (2002) 1207–1212.
[2] I. Guyon, J. Weston, S. Barnhill, V. Vapnik, Gene selection for cancer classification using support vector machines, Mach. Learn. 46 (2002) 389–422.
[3] H. Takahashi, H. Honda, A new reliable cancer diagnosis method using boosted fuzzy classifier with SWEEP operator method, J. Chem. Eng. Jpn. 38 (2005) 763–773.
[4] T.R. Golub, D.K. Slonim, P. Tamayo, C. Huard, M. Gaasenbeek, J.P. Mesirov, H. Coller, M.L. Loh, J.R. Downing, M.A. Caligiuri, C.D. Bloomfield, E.S. Lander, Molecular classification of cancer: class discovery and class prediction by gene expression monitoring, Science 286 (1999) 531–537.
[5] H. Takahashi, T. Kobayashi, H. Honda, Construction of robust prognostic predictors by using projective adaptive resonance theory as a gene filtering method, Bioinformatics 21 (2005) 179–186.
[6] D.J. Park, P.T. Vuong, S. de Vos, D. Douter, H.P. Koeffler, Comparative analysis of genes regulated by PML/RAR alpha and PLZF/RAR alpha in response to retinoic acid using oligonucleotide arrays, Blood 102 (2003) 3727–3736.
[7] S.L. Pomeroy, P. Tamayo, M. Gaasenbeek, L.M. Sturla, M. Angelo, M.E. McLaughlin, J.Y. Kim, L.C. Goumnerova, P.M. Black, C. Lau, J.C. Allen, D. Zagzag, J.M. Olson, T. Curran, C. Wetmore, J.A. Biegel, T. Poggio, S. Mukherjee, R. Rifkin, A. Califano, G. Stolovitzky, D.N. Louis, J.P. Mesirov, E.S. Lander, T.R. Golub, Prediction of central nervous system embryonal tumour outcome based on gene expression, Nature 415 (2002) 436–442.
[8] R.E. Schapire, The strength of weak learnability, Mach. Learn. 5 (1990) 197–227.
[9] Y. Freund, R. Schapire, A decision-theoretic generalization of online learning and an application to boosting, J. Comput. Syst. Sci. 55 (1997) 119–139.
[10] Y. Freund, Adaptive version of the boost by majority algorithm, Mach. Learn. 43 (2000) 293–318.
[11] J. Friedman, T. Hastie, R. Tibshirani, Additive logistic regression: a statistical view of boosting, Ann. Stat. 28 (2000) 337–407.

[12] S. Horikawa, T. Furuhashi, Y. Uchikawa, On fuzzy modeling using fuzzy neural networks with the back-propagation algorithm, IEEE Trans. Neural Networ. 3 (1992) 801–806.
[13] Y. Huang, Y. Li, Prediction of protein subcellular locations using fuzzy k-NN method, Bioinformatics 20 (2004) 21–28.
[14] V.N. Vapnik, A. Chervonenkis, A note on one class of perceptrons, Automat. Rem. Control 25 (1964) 821–837.
[15] T. Joachims, Making Large-scale SVM Learning Practical, MIT Press, Cambridge, 1999.
[16] H. Noguchi, T. Hanai, W. Takahashi, T. Ichii, M. Tanikawa, S. Masuoka, H. Honda, T. Kobayashi, Model construction for quality of beer and brewing process using FNN, Kagaku Kougaku Ronbunshu 25 (1999) 695–701.
[17] H. Noguchi, T. Hanai, H. Honda, L.C. Harrison, T. Kobayashi, Fuzzy neural network-based prediction of the motif for MHC class II binding peptides, J. Biosci. Bioeng. 92 (2001) 227–231.
[18] Y. Cao, J. Wu, Projective ART for clustering data sets in high dimensional spaces, Neural Networ. 15 (2002) 105–120.
[19] Y. Cao, J. Wu, Dynamics of projective adaptive resonance theory model: the foundation of PART algorithm, IEEE Trans. Neural Networ. 15 (2004) 245–260.
[20] P.G. Tan, Z. Xing, Z.Q. Li, Expression of cyclin D1 in brain gliomas and its significance, Ai Zheng 23 (2004) 63–65.
[21] J. Akervall, D.M. Kurnit, M. Adams, S. Zhu, S.G. Fisher, C.R. Bradford, T.E. Carey, Overexpression of cyclin D1 correlates with sensitivity to cis-platin in squamous cell carcinoma cell lines of the head and neck, Acta Otolaryngol. 124 (2004) 851–857.
[22] J.I. Park, C.J. Strock, D.W. Ball, B.D. Nelkin, The Ras/Raf/MEK/extracellular signal-regulated kinase pathway induces autocrine–paracrine growth inhibition via the leukemia inhibitory factor/JAK/STAT pathway, Mol. Cell. Biol. 23 (2003) 543–554.
[23] A. Frederick, M. Rolfe, M.I. Chiu, The human UNP locus at 3p21.31 encodes two tissue-selective, cytoplasmic isoforms with deubiquitinating activity that have reduced expression in small cell lung carcinoma cell lines, Oncogene 16 (1998) 153–165.

4-*S*-Cysteaminylphenol-loaded magnetite cationic liposomes for combination therapy of hyperthermia with chemotherapy against malignant melanoma

Akira Ito,[1] Masatake Fujioka,[2] Tatsuro Yoshida,[2] Kazumasa Wakamatsu,[3] Shosuke Ito,[3] Toshiharu Yamashita,[4] Kowichi Jimbow[4] and Hiroyuki Honda[2,5]

[1]Department of Chemical Engineering, Faculty of Engineering, Kyushu University, 744 Mototoka, Nishi-ku, Fukuoka 819-0395; [2]Department of Biotechnology, School of Engineering, Nagoya University, Furo-cho, Chikusa-ku, Nagoya 464-8603; [3]Department of Chemistry, Fujita Health University School of Health Sciences, Toyoake, Aichi 470-1192; [4]Department of Dermatology, Sapporo Medical University School of Medicine, South 1 West 17, Chuo-ku, Sapporo 060-8556, Japan

(Received June 28, 2006/Revised October 26, 2006/Accepted October 31, 2006/Online publication December 22, 2006)

Tyrosine analogs are good candidates for developing melanoma chemotherapies because melanogenesis is inherently toxic and expressed uniquely in melanocytic cells. The sulfur homolog of tyrosine, 4-*S*-cysteaminylphenol (4-*S*-CAP), was shown to be a substrate of melanoma tyrosinase and can cause selective cytotoxicity of melanocytes and melanoma cells. Previously, in order to improve the adsorption of magnetite nanoparticles to target cell surfaces, and generate heat in an alternating magnetic field (AMF) for cancer hyperthermia, we produced hyperthermia using magnetite cationic liposomes (MCL) that have a positive charge at the liposomal surface. In the present study, we constructed 4-*S*-CAP-loaded MCL (4-*S*-CAP/MCL), which act as a novel modality, combining melanoma-specific chemotherapy by 4-*S*-CAP with intracellular hyperthermia mediated by MCL. The 4-*S*-CAP/MCL exerted 4-*S*-CAP-mediated anticancer effects on B16 melanoma cells *in vitro* and *in vivo*. Moreover, after intratumoral injection of 4-*S*-CAP/MCL *in vivo*, the melanoma nodules were heated to 45°C under an AMF. Significantly higher therapeutic effects were observed in mice treated with the combination therapy mediated by 4-*S*-CAP/MCL plus AMF irradiation compared with mice treated with 4-*S*-CAP/MCL alone (without AMF) or mice treated with hyperthermia alone (MCL + AMF irradiation). These results suggest that this novel therapeutic tool is applicable to the treatment of malignant melanoma. (*Cancer Sci* 2007; 98: 424–430)

Hyperthermia is a promising approach to cancer therapy and has been used for many years to treat a wide variety of tumors in both experimental animals and patients.[1] In Japan, the most commonly used heating method in clinical settings is capacitive heating using a radiofrequency electric field.[2] An unavoidable technical problem with hyperthermia is the difficulty in heating only the local tumor region to the intended temperature without damaging the surrounding healthy tissue. Specifically, heating tumors by capacitive heating using a radiofrequency electric field is difficult because various factors, such as tumor size, position of electrodes, and adhesion of electrodes at uneven sites, influence the heating characteristics. Hyperthermia produced by heating mediators is a promising approach for specifically heating tumors without damaging normal tissues.[3] Magnetite nanoparticles have been used for hyperthermia treatment in an attempt to overcome this obstacle.[4–6] If magnetite nanoparticles can be made to accumulate only in tumor tissue, cancer-specific hyperthermia can be achieved by generating heat in an alternating magnetic field (AMF) due to hysteresis loss. In order to test this hypothesis, we developed magnetite cationic liposomes (MCL) as mediators of intracellular hyperthermia.[7–9] These cationic liposomes exhibit improved adsorption and accumulation in tumor cells, and have 10-fold higher affinity for tumor cells than neutrally charged magnetoliposomes,[7] thus suggesting that MCL are superior mediators of hyperthermia. We previously demonstrated the efficacy of MCL-mediated hyperthermia in animals with several cell lines, including T-9 rat glioma,[9] Os515 hamster osteosarcoma,[10] MM46 mouse mammary carcinoma,[11] PLS 10 rat prostate cancer,[12] and VX-7 squamous cell carcinoma in rabbit tongue.[13] Although MCL-mediated hyperthermia was found to be very effective for inducing complete tumor regression in transplantable tumor models, more powerful therapies are highly desired for cancer patients with malignancy.

Among the various forms of neoplasmas of the skin, malignant melanoma is the most invasive tumor. Various medical therapies, such as surgery, chemotherapy, radiotherapy and immunotherapy, are commonly used in the treatment of melanoma patients; however, none of these has proved sufficiently effective. Therefore, an effective protocol for the prevention and treatment of melanoma is needed urgently. Given this background, the combination of chemotherapy with MCL-mediated hyperthermia can be considered a possible strategy, because both magnetite nanoparticles and anticancer drugs can be encapsulated simultaneously into a liposome.

Tyrosine analogs are good candidates for developing melanoma chemotherapy because melanogenesis is inherently toxic and uniquely expressed in melanocytic cells. We introduced the use of phenolic thioether analogs of tyrosine for targeted melanoma chemotherapy based on the idea that the incorporation of sulfur would render the phenolics more cytotoxic by increased lipophilicity leading to increased uptake by cells, thus making them better substrates for tyrosinase.[14] Therefore, we synthesized the sulfur homolog of tyrosine, 4-*S*-cysteaminylphenol (4-*S*-CAP), in order to develop a targeted chemotherapy for malignant melanoma.[14,15] 4-*S*-CAP was found to be a substrate of melanoma tyrosinase and can cause selective cytotoxicity of melanocytes and melanoma cells.[16] In the present study, we constructed 4-*S*-CAP-loaded magnetite cationic liposomes (4-*S*-CAP/MCL) and investigated the feasibility of using them for combined melanoma-targeted chemotherapy and tumor-specific hyperthermia.

Materials and Methods

Cell lines and animal models. Mouse B16 melanoma cells were cultured in Dulbecco's modified Eagle's medium (Gibco BRL, Gaithersburg, MD, USA), supplemented with 10% fetal calf serum, 0.1 mg/mL streptomycin sulfate and 100 IU/mL potassium penicillin G. Normal human dermal fibroblasts (NHDF) were provided as frozen cells after primary culture by the supplier (Kurabo, Osaka, Japan), and were cultured in commercially available growth media (Medium106S; Kurabo) at 37°C in a humidified atmosphere of CO_2 and 95% air.

[5]To whom correspondence should be addressed. E-mail: honda@nubio.nagoya-u.ac.jp

doi: 10.1111/j.1349-7006.2006.00382.x

To prepare tumor-bearing mice, 8×10^5 B16 melanoma cells were injected subcutaneously into the right flank of C57BL/6 mice, which were anesthetized by intraperitoneal injection of pentobarbital (50 mg/kg bodyweight). Melanoma nodules that had grown to 5 mm in diameter were used for experiments. Tumor diameter was measured using calipers and the average size was determined by applying the following formula:

$$\text{Tumor size} = 0.5 \times (\text{length} + \text{width}),$$

where length and width were measured in mm.

Animal experiments were carried out according to the principles described in the 'Guide for the Care and Use of Laboratory Animals' prepared under the direction of the Prime Minister of Japan.

Analysis of the combined effect of 4-*S*-CAP and hyperthermic treatment. B16 cells were plated in six-well cell culture plates at 4×10^4 cells/well with experimental media containing 4-*S*-CAP at a concentration of 50 μM. The cells were then treated with hyperthermic treatment using a water bath. Hyperthermic treatment of cultured cells was carried out as in our previous report.[17] Briefly, the cells were heated to 42.5°C for 60 min by direct immersion of cell culture dishes in a temperature-controlled water bath. The temperature of the medium increased quickly and reached the intended temperature within 5 min. The temperature of the medium was monitored using a fiber optic thermometer probe (FX-9020; Anritsu Meter, Tokyo, Japan). Control cells were not treated with 4-*S*-CAP or hyperthermia.

The antiproliferative effect of the treatment was determined after a 2-day incubation period. The number of viable cells was evaluated by the trypan blue dye-exclusion method using a hemocytometer, and the relative cell number was calculated as follows:

$$\text{Relative cell number (\%)} = (\text{number of viable experimental cells/number of viable control cells}) \times 100.$$

The combined effect of 4-*S*-CAP and hyperthermia was evaluated using a method reported previously.[18] With [A], [B] and [A + B] representing the percentage cell viability for treatments A and B and the combination treatment A + B, the combined effects were defined as follows: synergistic, $[A + B] < [A] \times [B]/100$; additive, $[A + B] = [A] \times [B]/100$; subadditive, $[A] \times [B]/100 < [A + B] < [A]$, if $[A] < [B]$; interference, $[A] < [A + B] < [B]$, if $[A] < [B]$; and antagonistic, $[B] < [A + B]$, if $[A] < [B]$.

Preparation of 4-*S*-CAP/MCL. Magnetite nanoparticles (Fe_3O_4; average particle size, 10 nm) were the kind gift of Toda Kogyo (Hiroshima, Japan). 4-*S*-CAP was synthesized as described by Padgette *et al.*[19] For the preparation of 4-*S*-CAP/MCL, 0–32 mg of 4-*S*-CAP was added to a lipid mixture consisting of *N*-(α-trimethylammonioacetyl)-didodecyl-D-glutamate chloride (2.78 mg; Sogo Pharmaceutical, Tokyo, Japan), dilauroylphosphatidylcholine (6.64 mg; Sigma Chemical, St Louis, MO, USA) and dioleoylphosphatidyl-ethanolamine (5.58 mg; Sigma Chemical) dissolved in methanol (2 mL), and the mixture was dried down by evaporation for a minimum of 5 h. Then, the lipids containing 4-*S*-CAP were hydrated by vortexing with colloidal magnetite nanoparticles (20 mg/mL, 2 mL) and the liposomes were sonicated for 20 min (28 W). The size of the 4-*S*-CAP/MCL was measured using a dynamic light scattering spectrophotometer (FRAR 1000; Otsuka Electronics, Osaka, Japan).

Antiproliferative activity of 4-*S*-CAP in 4-*S*-CAP/MCL. B16 cells, or NHDF cells as a non-melanocytic control, were plated in six-well cell culture plates at 5×10^4 cells/well with experimental media containing 4-*S*-CAP/MCL at the indicated concentration. The antiproliferative activity was determined after the 2-day incubation period. The number of viable cells was measured by the trypan blue dye-exclusion method using a hemocytometer, and the relative cell number was calculated.

Uptake of 4-*S*-CAP/MCL by B16 cells. B16 cells were cultured to approximately 80% confluence before treatment with 4-*S*-CAP/MCL. Cells were then incubated with experimental media containing 4-*S*-CAP/MCL at a concentration of 43 μg magnetite/mL (4-*S*-CAP, 100 μM), and cells were incubated at 37°C with gentle shaking using a rotary shaker (SHK-320; Asahi Technoglass, Tokyo, Japan). After incubation for 24 h, the cells were washed twice with phosphate-buffered saline and harvested and the magnetite concentration was measured in accordance with our reported method.[7] Briefly, the harvested cells were dissolved completely in 0.2 mL of concentration HCl, after which 1 mL of 5% trichloroacetic acid was added. These mixtures were centrifuged in order to remove aggregates and the supernatants were measured by the potassium thiocyanate method.[20]

***In vitro* magnetite nanoparticle-induced hyperthermia.** An *in vitro* hyperthermia experiment using magnetite nanoparticles was carried out using our previously described method.[7] Briefly, B16 cells were cultured to approximately 80% confluence. Cells were then incubated with experimental media containing 4-*S*-CAP/MCL at a concentration of 43 μg magnetite/mL (4-*S*-CAP, 100 μM). At 24 h after the magnetite incorporation, the cells were collected in a microcentrifuge tube and centrifuged gently in order to form a cell pellet. The tube was then placed at the center of the coil of a high-frequency magnetic field generator (360 kHz, 120 Oe; Daiichi High Frequency, Tokyo, Japan). The temperature of the cell pellet was measured by inserting an optical fiber probe into its center, and the pellet was maintained at a constant temperature by manually tuning the strength of the magnetic field. The duration of the AMF irradiation was 30 min. During AMF irradiation, the temperature of the environment was maintained at 37°C. The treated cells were reseeded in a six-well cell culture plate at 2×10^4 cells/well. The number of viable cells was measured by the trypan blue exclusion method using a hemocytometer.

***In vivo* magnetite nanoparticle-induced hyperthermia.** When melanoma nodules grew to 5 mm in diameter, the tumor-bearing mice were separated into five groups (day 0). Mice in group I (control) were the non-treated control. Mice in groups II (MCL) and IV (MCL + AMF) received intratumoral injection of MCL (0.2 mL, 20 mg magnetite/mL). Mice in groups III (4-*S*-CAP/MCL) and V (4-*S*-CAP/MCL + AMF) received intratumoral injection of 4-*S*-CAP/MCL (0.2 mL; 20 mg/mL magnetite; 100 μM 4-*S*-CAP). At 1 day after the injection of MCL or 4-*S*-CAP/MCL (day 1), mice in groups IV (MCL + AMF) and V (4-*S*-CAP/MCL + AMF) were subjected to AMF for 30 min in a coil with a transistor inverter. Magnetic field frequency and intensity were 118 kHz and 384 Oe, respectively. Tumor and rectal temperatures were measured using an optical fiber probe. Subsequently, after the AMF irradiation, MCL or 4-*S*-CAP/MCL were again injected into the mice in groups II and IV or groups III and V, respectively. At 1 day after the second injection (day 2), mice in groups IV (MCL + AMF) and V (4-*S*-CAP/MCL + AMF) were again subjected to AMF for 30 min. During the injection of MCL or 4-*S*-CAP/MCL and AMF irradiation, tumor-bearing mice were anesthetized with pentobarbital sodium (50 mg/kg intraperitoneally).

For histological examination, the tumor was resected and fixed in a 10% formalin solution 24 h after hyperthermia. The specimens were fixed in 10% neutrally buffered formalin, and embedded in paraffin. Serial specimens were then prepared for histological examination, and were stained with hematoxylin and eosin (H&E).

Statistical analysis. Statistical analysis was carried out by the Mann–Whitney rank sum test calculated using WinSTAT statistical software (Light Stone International, Tokyo, Japan). Differences were considered to be statistically significant at $P < 0.05$.

Results

Combined effect of 4-*S*-CAP and hyperthermic treatment. Figure 1 shows the relative cell number for B16 cells on the second day

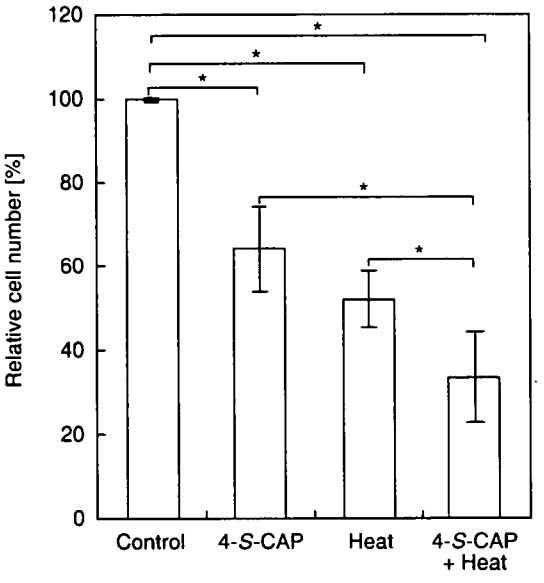

Fig. 1. Combined effects of 4-*S*-cysteaminylphenol (4-*S*-CAP) and heat treatment on B16 cell viability. B16 cells were treated with 4-*S*-CAP at 50 μM. Simultaneously, the cells were heated using a water bath at 42.5°C for 1 h. After the 2-day incubation period, antiproliferative effects were assessed as the relative cell number (%). Data and bars are mean ± SD of two independent experiments. $*P < 0.05$.

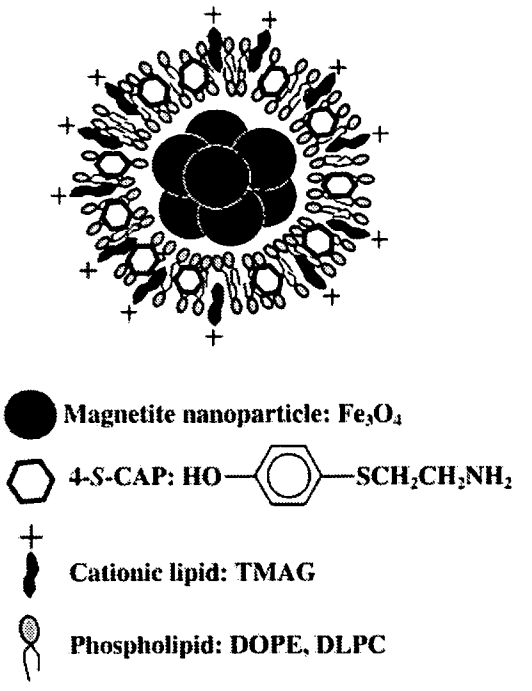

Fig. 2. Preparation of 4-*S*-cysteaminylphenol (4-*S*-CAP)/magnetite cationic liposomes (MCL). Illustration of 4-*S*-CAP/MCL is shown.

after hyperthermic treatment using a 42.5°C water bath for 60 min. For hyperthermic treatment alone, the relative cell number was 52.5 ± 6.6%. For 4-*S*-CAP (50 μM) treatment alone, the relative cell number was 64.4 ± 9.9%. When hyperthermic treatment was combined with 4-*S*-CAP treatment, the relative cell number decreased to 33.7 ± 10.6%. With [A], [B] and [A + B] representing the percentage cell viability for treatments of 4-*S*-CAP, heat and the combination treatment 4-*S*-CAP + heat, respectively, the combined effects were defined as follows: synergistic, [A + B] < [A] × [B]/100; additive, [A + B] = [A] × [B]/100; subadditive, [A] × [B]/100 < [A + B] < [A], if [A] < [B]; interference, [A] < [A + B] < [B], if [A] < [B]; and antagonistic, [B] < [A + B], if [A] < [B]. Here, [A + B] and [A] × [B]/100 were 33.7 ± 10.6% and 34.1 ± 9.5%, respectively. Because there was no significant difference ($P = 0.56$) between [A + B] and [A] × [B]/100, the combined effect of 4-*S*-CAP with heat was evaluated as additive effects.

Preparation of 4-*S*-CAP-loaded MCL. Because the combination of 4-*S*-CAP and hyperthermia has an additive effect, we constructed 4-*S*-CAP/MCL (Fig. 2) and investigated whether 4-*S*-CAP/MCL can combine 4-*S*-CAP-mediated chemotherapy with MCL-induced hyperthermia. The size distribution of 4-*S*-CAP/MCL with various 4-*S*-CAP contents was measured using a dynamic light-scattering spectrophotometer (Fig. 3). For MCL without 4-*S*-CAP, the peak in the particle size distribution was 124.5 ± 0.95 nm (the mean ± SD of three independent experiments). The average size of 4-*S*-CAP/MCL increased drastically when the 4-*S*-CAP concentration exceeded 100 μM. When the 4-*S*-CAP concentration exceeded 100 μM, the dispersibility of 4-*S*-CAP/MCL was extremely low and precipitation of 4-*S*-CAP/MCL was observed. Therefore, 4-*S*-CAP/MCL at 100 μM of 4-*S*-CAP concentration was used in the following *in vivo* experiments.

Antiproliferative activity of 4-*S*-CAP in 4-*S*-CAP/MCL. Figure 4a shows the antiproliferative effects of different concentrations of 4-*S*-CAP/MCL on B16 cells. The dose–response curve showed a dose-dependent antiproliferative effect for 4-*S*-CAP in 4-*S*-CAP/MCL, with the maximum effects achieved using a concentration of 400 μM (46.6 ± 0.9% of relative cell number), which was comparable to the cytotoxicity of free 4-*S*-CAP (inhibition

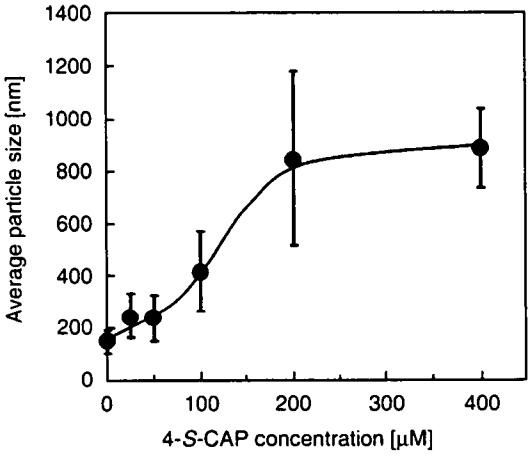

Fig. 3. Relationship between 4-*S*-cysteaminylphenol (4-*S*-CAP) concentration and liposome size of 4-*S*-CAP/magnetite cationic liposomes (MCL). The size of the 4-*S*-CAP/MCL was measured using a dynamic light scattering spectrophotometer. Data and bars are mean ± SD of three independent experiments.

concentration [IC_{50}] IC_{50} of 507 μM) toward B16 melanoma cells.[21] Figure 4b shows the time course of the relative cell number when B16 or NHDF cells were treated with 100 μM 4-*S*-CAP/MCL. The relative cell number for B16 cells decreased linearly to 60% during the 2-day culture period. In contrast, non-melanocytic NHDF cells showed no decrease in relative cell number 1 day after 4-*S*-CAP/MCL treatment, with only slight antiproliferative effects (15% decrease in the relative cell number) observed on day 2. These results indicate that 4-*S*-CAP in 4-*S*-CAP/MCL had an antiproliferative effect on B16 cells, although 4-*S*-CAP was less toxic to non-melanocytic NHDF cells, an observation that corresponds to previous reports.[22]

Uptake of magnetite nanoparticles by B16 cells and *in vitro* hyperthermia. Next, in order to assess the feasibility of magnetite nanoparticle-mediated hyperthermia *in vitro*, we investigated whether 4-*S*-CAP/MCL

doi: 10.1111/j.1349-7006.2006.00382.x

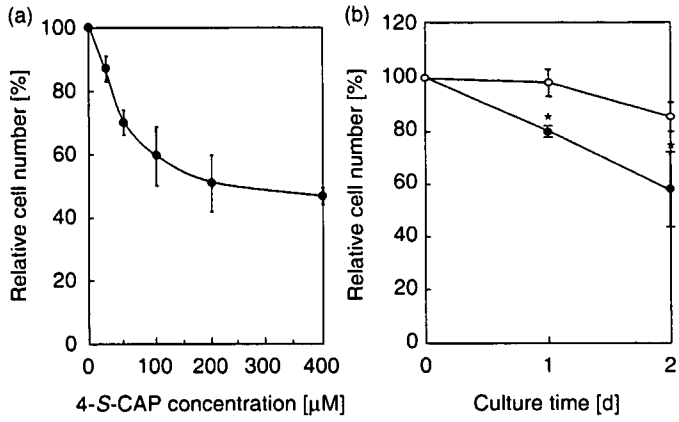

Fig. 4. Antiproliferative activity of 4-*S*-cysteaminylphenol (4-*S*-CAP) mediated by 4-*S*-CAP/magnetite cationic liposomes (MCL). (a) B16 cells were treated with different concentrations of 4-*S*-CAP/MCL (4-*S*-CAP, 0–400 μM). After the 2-day incubation period, antiproliferative effects were assessed as the relative cell number (%). Data and bars are mean ± SD of three independent experiments. (b) B16 (●) and normal human dermal fibroblasts (NHDF) (○) cells were treated with 4-*S*-CAP/MCL at 100 μM 4-*S*-CAP, and the relative cell number was assessed on days 1 and 2. Data and bars are mean ± SD of three independent experiments. $*P < 0.05$.

were incorporated into B16 cells. The uptake of magnetite nanoparticles by B16 cells is shown in Fig. 5a. Magnetite nanoparticles in 4-*S*-CAP/MCL were incorporated into B16 cells, and the amount of uptake was 18.4 ± 1.0 pg magnetite/cell after 24 h, which was comparable to that of MCL (15.0 ± 0.4 pg magnetite/cell).

We then investigated whether AMF irradiation generated heat in B16 cells treated with 4-*S*-CAP/MCL, and observed intracellular hyperthermia *in vitro*. Figure 5b shows the temperature profile of cell pellets treated with 4-*S*-CAP/MCL during AMF irradiation at 360 kHz and 120 Oe. Heat was generated in B16 cells incorporating magnetite nanoparticles. The temperature of these cells rose quickly and reached 43.0°C, which is an effective temperature for hyperthermia treatment, and was then maintained at that temperature for 30 min by controlling the intensity of the AMF. In contrast, in non-treated cells (0 pg magnetite/cell), the temperature increased only 2°C during the AMF irradiation. Figure 5c shows the viable cell number after the AMF irradiation. When the cells were treated with 4-*S*-CAP/MCL alone (without irradiation; 4-*S*-CAP/MCL, 100 μM), the viable cell number decreased to approximately half of that for non-treated cells. Moreover, when the cells were treated with 4-*S*-CAP/MCL plus AMF irradiation, the viable cell number decreased drastically for 1 day and thereafter cells grew again, resulting in an apparently smaller number than with 4-*S*-CAP/MCL alone (without irradiation).

***In vivo* hyperthermic treatment using 4-*S*-CAP/MCL.** For hyperthemic treatment *in vivo*, 4-*S*-CAP/MCL was injected into the tumor and AMF was applied to the whole body of the mouse. Figure 6a shows the tumor surface and rectal temperatures during AMF irradiation. Tumor temperature increased rapidly to 45°C within 3 min and was then maintained for 30 min by controlling the AMF intensity. In contrast, the temperature in the rectum showed only a limited increase during irradiation. These temperature profiles for 4-*S*-CAP/MCL-induced hyperthermia were comparable to those of MCL-induced hyperthermia (data not shown). No serious burns or damage were observed in all mice treated with magnetite-mediated hyperthermia.

For B16 melanoma, the therapeutic effects of the 4-*S*-CAP/MCL-induced combination of chemotherapy and hyperthermia

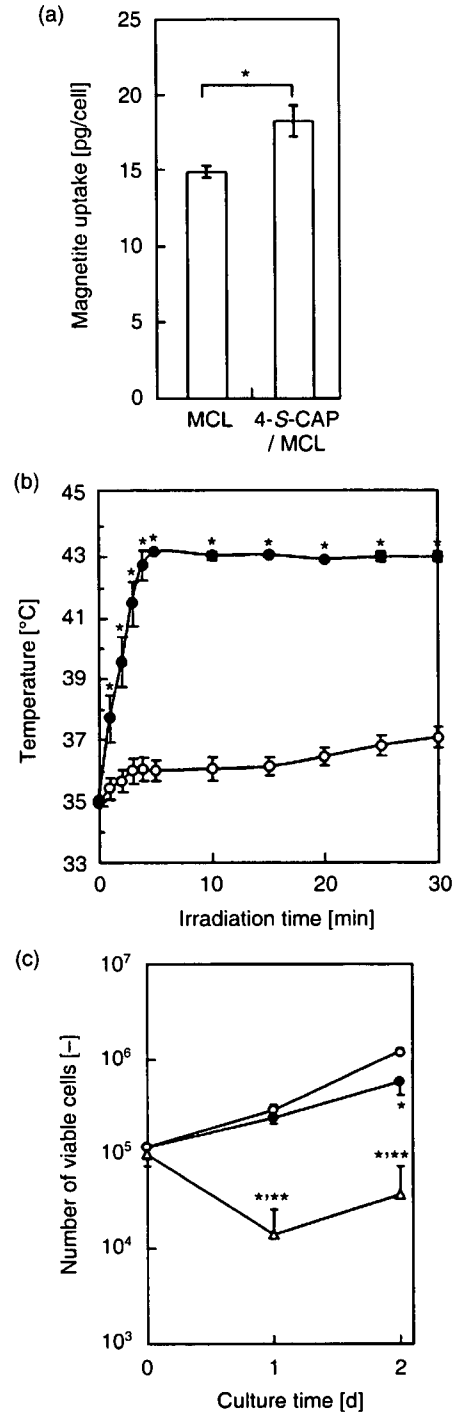

Fig. 5. *In vitro* hyperthermia induced by 4-*S*-cysteaminylphenol (4-*S*-CAP)/magnetite cationic liposomes (MCL). (a) Uptake of magnetite nanoparticles into B16 cells at 24 h after addition of MCL or 4-*S*-CAP/MCL. Percentage magnetite uptake was evaluated. Data and bars are mean ± SD of three independent experiments ($*P < 0.05$). (b) Temperature increase in cell pellets treated with 4-*S*-CAP/MCL during alternating magnetic field (AMF) irradiation. B16 cells with (●) or without (○) 4-*S*-CAP/MCL were irradiated with AMF for 30 min. Data and bars are mean ± SD of three independent experiments ($*P < 0.05$). (c) *In vitro* antiproliferation effects of 4-*S*-CAP/MCL after AMF irradiation. After the AMF irradiation, cells were reseeded and the number of viable cells was measured on the indicated day by the trypan blue exclusion method using a hemocytometer. (○) Control B16 cells; (●) B16 cells with 4-*S*-CAP/MCL; and (△) B16 cells treated with 4-*S*-CAP/MCL and AMF irradiation. Data and bars are mean ± SD of three independent experiments. $*P < 0.05$, significantly different from control group (non-treated B16 cells); $**P < 0.05$, significantly different from 4-*S*-CAP/MCL group (4-*S*-CAP/MCL alone).

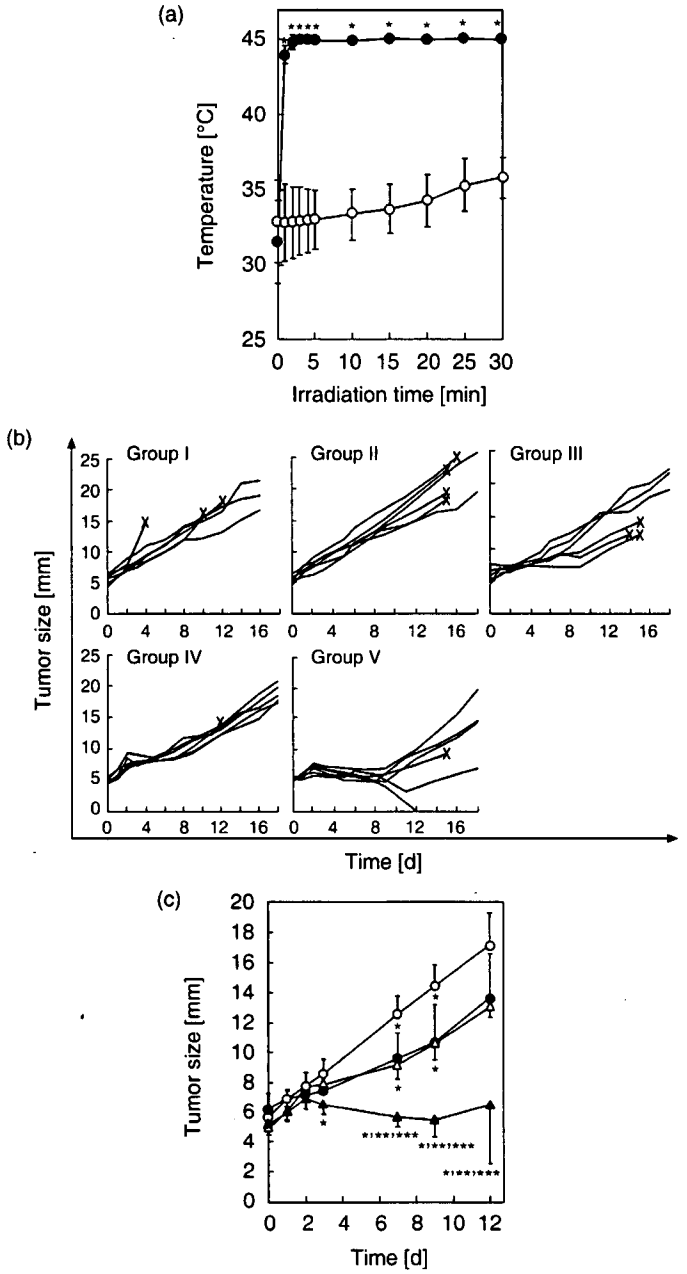

Fig. 6. *In vivo* hyperthermia using 4-*S*-cysteaminylphenol (4-*S*-CAP)/magnetite cationic liposomes (MCL). Schema of the therapeutic experiment. (a) Temperature increase in melanoma nodules treated with 4-*S*-CAP/MCL during alternating magnetic field (AMF) irradiation. 4-*S*-CAP/MCL containing 4 mg magnetite were injected directly into subcutaneous B16 tumors with diameters of 5 mm, which were then irradiated with an AMF for 30 min. Tumor and rectal temperatures were measured using optical fiber probes. (●) Tumor; (○) rectum. Each point represents the mean ± SD of five mice. $*P < 0.01$. (b) Therapeutic effects of 4-*S*-CAP/MCL on B16 tumors. Each line represents tumor growth in a single mouse ($n = 6$). Crosses (×) indicate when each mouse died. (c) Comparison of each group in the first 12 days after treatment. (○) Group II; (●) group III; (△) group IV; (s) group V. Each point represents the mean ± SD of six mice. $*P < 0.05$, significantly different from group II (MCL alone); $**P < 0.05$, significantly different from group III (4-*S*-CAP/MCL alone); $***P < 0.05$, significantly different from group IV (MCL + AMF).

were assessed. Figure 6b shows the time course of tumor growth in each mouse, and the comparison of tumor growth kinetics in each group in the first 12 days is shown in Fig. 6c. In groups I (control) and II (MCL), tumors grew progressively and some mice died from pulmonary metastases (data not shown). In

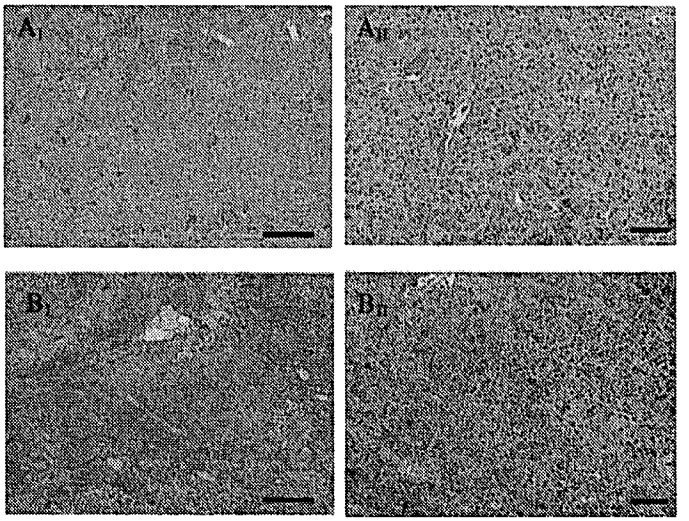

Fig. 7. Pathological features of the tumor in representative mice treated with hyperthermia using 4-*S*-cysteaminylphenol (4-*S*-CAP)/magnetite cationic liposomes (MCL). Tumors of mice in the control group (groups I, A-I and A-II) and 4-*S*-CAP/MCL-induced hyperthermia treatment group (groups IV, B-I and B-II) were stained with hematoxylin and eosin. Scale bars in I and II are 200 μm and 50 μm, respectively.

groups III (4-*S*-CAP/MCL), in which mice received 4-*S*-CAP/MCL alone (without AMF irradiation), and IV (MCL + AMF), in which mice received MCL-induced hyperthermia, tumor growth was slightly but significantly suppressed on days 7 and 9, and thereafter tumors grew progressively. In contrast, in group V (4-*S*-CAP/MCL + AMF), in which mice received 4-*S*-CAP/MCL and AMF irradiation, tumor growth was strongly suppressed in the first 12 days (Fig. 6c), and 17% (1/6) of subcutaneous tumors regressed completely (Fig. 6b). Histological examination of the tumors was done by H&E staining (Fig. 7). Severe necrosis with hemorrhage was observed, and many dead cells with condensed nuclei were seen, as shown in Fig. 7.

Discussion

In the present study, we examined the combination effect of 4-*S*-CAP treatment and hyperthermia on B16 melanoma cells, and demonstrated that the combination therapy has an additive effect (Fig. 1). In normal melanocytes and malignant melanoma cells, the specific enzyme tyrosinase catalyzes the oxidative conversion of L-tyrosine to melanin pigments.[23] 4-*S*-CAP is a good substrate for tyrosinase, and an oxidized form binds to sulphydryl enzymes.[24] With respect to the mechanism of cytotoxicity, dihydro-1,4-benzothiazine-6,7-dione, a metabolite of 4-*S*-CAP, deprives melanoma cells of reduced glutathione and may inactivate SH enzymes essential for DNA synthesis and cell proliferation by covalent binding through their cysteine residues, thereby exerting melanocytotoxicity.[21] Thus, cytotoxicity of 4-*S*-CAP depends mostly on reactive oxygen species (ROS). Similarly to 4-*S*-CAP activities in melanoma cells, hyperthermia can promote the formation of free radicals and related ROS from metabolic pathways, and these ROS may result in some cellular injury.[25] We speculate that ROS played an important role in the additive effect of the combined 4-*S*-CAP treatment and hyperthermia on melanoma cells; therefore, further research is required in order to elucidate the mechanism.

In the case of a superficial tumor, such as melanoma, a simple heat mediator is desirable for the clinical application of hyperthermia. Previously, we confirmed hyperthermic effects on B16

doi: 10.1111/j.1349-7006.2006.00382.x

melanoma using MCL injected directly into the tumor.[26] MCL uptake by cells in the injection site was much higher than that of magnetoliposomes whose liposomal surface had neutral charge, because MCL can electrostatically interact with the negative-charged phospholipid membrane of cells,[7] resulting in retention at the injection site. Thus, in a drug-targeting modality for melanoma, the use of 4-*S*-CAP/MCL is appropriate because superficial tumors can be treated with intratumoral injection of 4-*S*-CAP/MCL. Therefore, we used 4-*S*-CAP/MCL in order to heat the tumoral region and minimize heating of the surrounding healthy tissue. As shown in Fig. 6a, during hyperthermia using 4-*S*-CAP/MCL, tumor temperature reached 45°C rapidly, whereas rectal temperature remained at 38°C. These results indicate that using 4-*S*-CAP/MCL allows the application of hyperthermia to specific tumor tissue and that accurate control of the tumor temperature is possible by manipulating the magnetic field intensity. In this study, we set the tumor temperature at 45°C; however, this was insufficient to completely destroy the malignant melanoma. Our hyperthermia system can be carried out at higher temperatures and can be conducted repeatedly without damaging healthy tissue. For example, complete regression of B16 melanoma was observed in 90% of mice using MCL-induced hyperthermia at 46°C applied once daily for 2 days.[26] In the present study, we set the temperature at 45°C in order to examine the effects of combining hyperthermia with 4-*S*-CAP-madiated chemotherapy.

A major advantage of hyperthermia is that it has few side effects. In contrast to chemotherapy, hyperthermic effects are independent of cell lines and animals.[9–13] Furthermore, hyperthermic effects on cancer cells are caused mainly by physical damage, and differences in sensitivities to hyperthermia are negligible, especially at higher temperatures.[27,28] Therefore, when magnetite nanoparticles are internalized into tumor cells, the hyperthermic effect should be independent of cell type. However, in the case of repeated injection of 4-*S*-CAP/MCL, the toxicity of 4-*S*-CAP/MCL may become an important issue in a clinical trial. For MCL, in our preliminary study, the toxicity of a single administration of MCL solution (33 mg magnetite, intraperitoneally) was investigated. MCL accumulated mostly in the liver and spleen of mice, but none of the five observed mice died after MCL injection.[29] In the present study, 8 mg magnetite was used, which was much less than that used in the preliminary examination (33 mg). The 4-*S*-CAP was synthesized as an antimelanoma agent that is selectively toxic to the *in vivo* melanocytes engaged in melanin synthesis,[30,31] but not to the melanocytes and keratinocytes of albino mice.[31] However, a study by Padgette *et al.* has shown that 4-*S*-CAP is a good substrate of plasma monoamine oxidase, as well as tyrosinase.[19] The cytotoxicity of 4-*S*-CAP to cultured cells may be partly mediated by the aldehyde formed by oxidative deamination.[32] In the present study, non-melanocytic NHDF cells showed a slight decrease in relative cell number (decrease of 15%; Fig. 4b), suggesting that 4-*S*-CAP induced tyrosinase-independent toxicity. However, the mechanism of this tyrosinase-independent toxicity remains to be clarified. Taken together, these findings indicate that 4-*S*-CAP/MCL toxicity should be fully investigated before clinical application.

In conclusion, the promising results of the present study warrant further investigation of new modalities using 4-*S*-CAP/MCL, with the long-term goal of future application in the treatment of malignant melanoma in humans.

Acknowledgments

The authors would like to thank Toda Kogyo Co. for supplying the magnetite. This work was partially supported by a Health and Labour Sciences Research Grant-in-Aid for Research on Advanced Medical Technology from the Ministry of Health, Labour and Welfare, a Grant-in-Aid for University Start-Up Creation Support System, and a 21st Century COE Program 'Nature-Guided Materials Processing' grant from the Ministry of Education, Culture, Sports, Science, and Technology of Japan.

References

1 Van der Zee J. Heating the patient: a promising approach? *Annu Oncol* 2002; **13**: 1173–84.
2 Abe M, Hiraoka M, Takahashi M *et al.* Multi-institutional studies on hyperthermia using an 8-MHz radiofrequency capacitive heating device (Thermotron RF-8) in combination with radiation for cancer therapy. *Cancer* 1986; **58**: 1589–95.
3 Moroz P, Jones SK, Gray BN. Magnetically mediated hyperthermia: current status and future directions. *Int J Hyperthermia* 2002; **18**: 267–84.
4 Jordan A, Wust P, Fahling H, John W, Hinz A, Felix R. Inductive heating of ferrimagnetic particles and magnetic fluids: physical evaluation of their potential for hyperthermia. *Int J Hyperthermia* 1993; **9**: 51–68.
5 Minamimura T, Sato H, Kasaoka S *et al.* Tumor regression by inductive hyperthermia combined with hepatic embolization using dextran magnetite-incorporated microspheres in rats. *Int J Oncol* 2000; **16**: 1153–8.
6 Shinkai M, Matsui M, Kobayashi T. Heat properties of magnetoliposomes for local hyperthermia. *Jpn J Hyperthermic Oncol* 1994; **10**: 168–77.
7 Shinkai M, Yanase M, Honda H, Wakabayashi T, Yoshida J, Kobayashi T. Intracellular hyperthermia for cancer using magnetite cationic liposomes: *in vitro* study. *Jpn J Cancer Res* 1996; **87**: 1179–83.
8 Yanase M, Shinkai M, Honda H, Wakabayashi T, Yoshida J, Kobayashi T. Intracellular hyperthermia for cancer using magnetite cationic liposomes: *ex vivo* study. *Jpn J Cancer Res* 1997; **88**: 630–2.
9 Yanase M, Shinkai M, Honda H, Wakabayashi T, Yoshida J, Kobayashi T. Intracellular hyperthermia for cancer using magnetite cationic liposomes: an *in vivo* study. *Jpn J Cancer Res* 1998; **89**: 463–9.
10 Matsuoka F, Shinkai M, Honda H, Kubo T, Sugita T, Kobayashi T. Hyperthermia using magnetite cationic liposomes for hamster osteosarcoma. *Biomagn Res Technol* 2004; **25**: 3.
11 Ito A, Tanaka K, Honda H, Abe S, Yamaguchi H, Kobayashi T. Complete regression of mouse mammary carcinoma with a size greater than 15 mm by frequent repeated hyperthermia using magnetite nanoparticles. *J Biosci Bioeng* 2003; **96**: 364–9.
12 Kawai N, Ito A, Nakahara Y *et al.* Anticancer effect of hyperthermia on prostate cancer mediated by magnetite cationic liposomes and immune-response induction in transplanted syngeneic rats. *Prostate* 2005; **64**: 373–81.
13 Matsuno H, Tohnai I, Mitsudo K *et al.* Interstitial hyperthermia using magnetite cationic liposomes to inhibit tumor growth of VX-7 transplanted tumor in rabbit tongue. *Jpn J Hyperthermic Oncol* 2001; **17**: 141–50.
14 Miura S, Ueda T, Jimbow K, Ito S, Fujita K. Synthesis of cysteinylphenol, cysteaminylphenol, and related compounds, and *in vivo* evaluation of antimelanoma effect. *Arch Dermatol Res* 1987; **279**: 219–25.
15 Yamada I, Seki S, Matsubara O, Ito S, Suzuki S, Kasuga T. The cytotoxicity of cysteinylcatechols and related compounds to human melanoma cells *in vitro*. *J Invest Dermatol* 1987; **88**: 538–40.
16 Minamitsuji Y, Toyofuku K, Sugiyama S, Yamada K, Jimbow K. Sulfur containing tyrosine analogs can cause selective melanocytotoxicity involving tyrosinase-mediated apoptosis. *J Invest Dermatol Symp Proc* 1999; **4**: 130–6.
17 Ito A, Shinkai M, Honda H, Wakabayashi T, Yoshida J, Kobayashi T. Augmentation of MHC class I antigen presentation via heat shock protein expression by hyperthermia. *Cancer Immunol Immunother* 2001; **50**: 515–22.
18 Valeriote F, Lin H. Synergistic interaction of anticancer agents: a cellular perspective. *Cancer Chemother Rep* 1975; **59**: 895–900.
19 Padgette SR, Herman HH, Han JH, Pollock SH, May SW. Antihypertensive activities of phenyl aminoethyl sulfides, a class of synthetic substrates for dopamine β-hydroxylase. *J Med Chem* 1984; **27**: 1354–7.
20 Owen CS, Sykes NL. Magnetic labeling and cell sorting. *J Immunol Methods* 1984; **73**: 41–8.
21 Hasegawa K, Ito S, Inoue S, Wakamatsu K, Ozeki H, Ishiguro I. Dihydro-1,4-benzothiazine-6,7-dione, the ultimate toxic metabolite of 4-*S*-cysteaminylphenol and 4-*S*-cysteaminylcatechol. *Biochem Pharmacol* 1997; **53**: 1435–44.
22 Parsons PG, Favier D, McEwan M, Takahashi H, Jimbow K, Ito S. Action of cysteaminylphenols on human melanoma cells *in vivo* and *in vitro*: 4-*S*-cysteaminylphenol binds protein disulphide isomerase. *Melanoma Res* 1991; **1**: 97–104.
23 Prota G. *Melanins and Melanogenesis*. New York: Academic Press, 1992.
24 Ito S, Kato T, Ishikawa K, Kasuga T, Jimbow K. Mechanism of selective toxicity of 4-*S*-cysteinylphenol and 4-*S*-cysteaminylphenol to melanocytes. *Biochem Pharmacol* 1987; **36**: 2007–11.
25 Venkataraman S, Wagner BA, Jiang X *et al.* Overexpression of manganese superoxide dismutase promotes the survival of prostate cancer cells exposed to hyperthermia. *Free Radic Res* 2004; **38**: 1119–32.

26 Suzuki M, Shinkai M, Honda H, Kobayashi T. Anticancer effect and immune induction by hyperthermia of malignant melanoma using magnetite cationic liposomes. *Melanoma Res* 2003; **13**: 129–35.
27 Kano E, Miyakoshi J, Sugahara T. Difference in sensitivities to hyperthermia and ionizing radiation of various mammalian cell stress *in vitro*. In: Streffer C, Van Beuninen D, Dietzel F *et al.*, eds. *Cancer Therapy by Hyperthermia and Radiation*. Baltimore-Munich: Urban and Schwarzenberg, 1978: 188–90.
28 Kano E, Miyakoshi J, Furukawa M *et al.* Effects of hyperthermia at 50 degrees C on V-79 cells *in vitro*. *J Radiat Res (Tokyo)* 1982; **23**: 218–27.
29 Ito A, Nakahara Y, Tanaka K, Kuga Y, Honda H, Kobayashi T. Time course of biodistribution and heat generation of magnetite cationic liposomes in mouse model. *Jpn J Hyperthermic Oncol* 2003; **19**: 151–9.
30 Ito Y, Jimbow K, Ito S. Depigmentation of black guinea pig skin by topical application of cysteaminylphenol, cysteinylphenol, and related compounds. *J Invest Dermatol* 1987; **88**: 77–82.
31 Ito Y, Jimbow K. Selective cytotoxicity of 4-*S*-cysteaminylphenol on follicular melanocytes of the black mouse: rational basis for its application to melanoma chemotherapy. *Cancer Res* 1987; **47**: 3278–84.
32 Inoue S, Ito S, Wakamatsu K, Jimbow K, Fujita K. Mechanism of growth inhibition of melanoma cells by 4-*S*-cysteaminylphenol and its analogues. *Biochem Pharmacol* 1990; **39**: 1077–83.

doi: 10.1111/j.1349-7006.2006.00382.x

ARTICLE

BIOTECHNOLOGY and BIOENGINEERING

Construction of Multi-Layered Cardiomyocyte Sheets Using Magnetite Nanoparticles and Magnetic Force

Kazunori Shimizu,[1,2] Akira Ito,[1] Jong-Kook Lee,[3] Tatsuro Yoshida,[1] Keiko Miwa,[3] Hisaaki Ishiguro,[4] Yasushi Numaguchi,[4] Toyoaki Murohara,[4] Itsuo Kodama,[3] Hiroyuki Honda[1]

[1]Department of Biotechnology, School of Engineering, Nagoya University, Nagoya, Japan; telephone: +81 52 7893215; fax: +81 52 7893214; e-mail: honda@nubio.nagoya-u.ac.jp

[2]Research Fellow of the Japan Society for the Promotion of Science (JSPS Research Fellow) 8 Ichibancho, Chiyoda-ku, Tokyo, Japan

[3]Department of Circulation, Research Institute of Environmental Medicine, Nagoya University, Nagoya, Japan

[4]Department of Cardiology, Nagoya University Graduate School of Medicine, Nagoya, Japan

Received 4 April 2006; accepted 19 June 2006

Published online 24 July 2006 in Wiley InterScience (www.interscience.wiley.com). DOI 10.1002/bit.21094

ABSTRACT: Heart tissue engineering requires construction of three-dimensional (3-D) tissues composed of cardiomyocytes (CMs) that are tightly connected to each other. The aim of this study was to construct "scaffold-less" multi-layered 3-D CM sheets using magnetic force-based tissue engineering (Mag-TE) and to evaluate the cell-to-cell functional connections within the CM sheets. Original magnetite cationic liposomes (MCLs) with a positive surface charge (which facilitate adsorption to the target cell surface) were taken up by CMs that were isolated from 2-day-old Wistar rats. When MCLs were added to the medium of CMs at magnetite concentrations of 25, 50, and 100 pg per cell, subsequent measurements showed that 7.2, 13.2, and 27.3 pg of magnetite were taken up per cell, respectively, after 4 h incubation at 37°C. Further, no toxicity was observed after a 24 h incubation period. Using magnetically labeled CMs (magnetite concentration, 100 pg/cell), multi-layered CM sheets were constructed. Immunofluorescent staining of connexin43 demonstrated the presence of gap junctions within the CM sheets that were constructed by Mag-TE. Moreover, electrical connections within the CM sheets constructed by Mag-TE were confirmed using extracellular potential mapping. These results indicate that Mag-TE is a viable methodology for heart tissue engineering.

Biotechnol. Bioeng. 2007;96: 803–809.

KEYWORDS: magnetite nanoparticles; liposomes; tissue engineering; cardiomyocytes; 3-D cells culture

Introduction

Heart failure is the leading cause of death in industrialized countries. Although heart transplantation is a definitive solution for patients with end-stage heart failure, this strategy is limited by the relative lack of organ donors and by the complications associated with subsequent immunosuppressive treatments that are required to avoid rejection of the transplanted tissue.

Tissue engineering represents another alternative for the treatment of end-stage heart failure (Langer and Vacanti, 1993), and several tissue engineering approaches are being investigated in the context of cardiac repair (Zammaretti and Jaconi, 2004; Zimmermann et al., 2004). The most common approach used thus far is the seeding of cardiomyocytes (CMs) into biodegradable porous synthetic or natural polymers (Akins et al., 1999; Carrier et al., 1999; Papadaki et al., 2001). While simulation of native cardiac tissue requires dense packing of CMs and electrical connections between cells in the form of gap junctions, the scaffolds used to construct these tissues attenuate cell-to-cell connections and tend to induce an inflammatory reaction due to scaffold biodegradation. Thus, investigators have proposed the use of novel tissue-engineering methodologies for construction of three-dimensional (3-D) cardiac tissue without scaffolds.

Magnetite (Fe_3O_4) particles have been used for cell sorting and bioseparation (Miltenyi et al., 1990; Moore et al., 1998;

Correspondence to: H. Honda

Contract grant sponsor: Ministry of Education, Sports, Science, and Technology, Japan

Contract grant numbers: 17760622; 17066003; 18048024; 18038021

Radbruch et al., 1994), and our group reported that magnetite cationic liposomes (MCLs), which are cationic liposomes containing 10-nm magnetite nanoparticles, improve the accumulation of magnetite nanoparticles in target cells via electrostatic interaction between MCLs and the cell membrane (Shinkai et al., 1996). On the basis of these data, we previously proposed a "magnetic force-based tissue engineering (Mag-TE)" methodology that uses magnetic force and cells that were magnetically labeled with MCLs (Ito et al., 2004c, 2005b,c; Shimizu et al., 2005). Previous studies (Ito et al., 2004a, 2005a; Shimizu et al., 2006) showed that desmosomes were present within the keratinocyte sheets constructed by Mag-TE (Ito et al., 2004a). However, further experiments were needed to examine the "functional" connections within the sheets constructed by Mag-TE. Therefore, the goal of this study was to construct "scaffold-less" multi-layered 3-D CM sheets using Mag-TE and to evaluate the cell-to-cell functional connections within the CM sheets.

Materials and Methods

Neonatal Cardiomyocyte (CM) Isolation

Neonatal CMs were isolated using a neonatal CM isolation system (Worthington Biochemical, Lakewood, NJ), according to the manufacturer's instructions with some modifications. Briefly, 2-day-old Wistar rats (Japan SLC, Inc., Hamamatsu, Japan) were sacrificed, and the left ventricles were excised. The tissues were minced with small scissors to ≤ 1 mm^3 pieces in sterile calcium- and magnesium-free Hank's balanced salt solution (Worthington Biochemical) and incubated for 16–20 h at 4°C with trypsin (50 μg/mL, Worthington Biochemical). The tissues were transferred to a T25 flask with an air transmittable cap (Asahi Techno Glass, Chiba, Japan), and 1 mL of trypsin inhibitor (2,000 μg/mL, Worthington Biochemical) was then added. After collagenase addition (1,500 U, Worthington Biochemical), the flask was gently mixed and incubated for 40 min at 37°C in a humidified atmosphere (5% CO_2 and 95% air). The resulting pellet was resuspended in Medium 199 (Invitrogen, Carlsbad, CA) containing 10% fetal bovine serum (FBS; Sigma, St. Louis, MO), 2.7 mM glucose, 0.1 mg/mL streptomycin sulfate, and 100 U/mL potassium penicillin G (Invitrogen), and pre-plated to allow preferential attachment of non-CMs, such as fibroblasts. After 1 h incubation, the non-adherent cells were collected and plated onto 35-mm cell culture dish (BD Primaria™, BD Bioscience, Billerica, MA). Six sub-confluent dishes were obtained from 10 hearts. In our previous study, the purity of the isolated CM population characterized by immunolabeling against anti-actin antibody was >97%. (Inoue et al., 2004). Medium exchange was performed every day, and cells cultured for 4 days were used as CMs in the present study.

Preparation of Magnetic Cationic Liposomes (MCLs)

Magnetite (Fe_3O_4; average particle size, 10 nm) was used as the core of the MCLs and was obtained from Toda Kogyo (Hiroshima, Japan). MCLs were fabricated as previously described (Shinkai et al., 1996). Briefly, colloidal magnetite and a lipid mixture consisting of *N*-(α-trimethylammonioacetyl)-didodecyl-D-glutamate chloride (TMAG, a cationic lipid, Sogo pharmaceutical, Tokyo, Japan), dilauroylphosphatidyl-choline (DLPC, Sigma-Aldrich, St. Louis, MS), and dioleoylphosphatidyl-ethanolamine (DOPE, Avanti Polar Lipids, Inc., Alabaster, AL) in a 1:2:2 molar ratio was used. The average MCL particle size was 150 nm, as measured by a dynamic light scattering spectrophotometer (FRAR 700S, Otsuka Electronics, Osaka, Japan).

MCL Uptake by CMs

Uptake of MCLs by CMs was examined as previously described (Shinkai et al., 1996). Briefly, CMs were isolated and cultured in 35-mm cell culture dishes with 3 mL of culture medium for 4 days, as described above. The medium was then replaced with the MCL-containing medium (net magnetite concentration, 25, 50, and 100 pg/cell), and CMs were incubated. To assay magnetite uptake, cells were sampled periodically, and the iron concentration within cells was measured using the potassium thiocyanate method (Owen and Sykes, 1984). To examine the effects of MCL uptake on cell viability, cells were counted using the dye-exclusion method with trypan blue. Percentage of viable cells was determined by the equation: percentage of viable cells = (number of viable CMs at the indicated time/number of viable CMs at 0 h) × 100.

Construction of CM Sheets by Mag-TE

CMs sheets were constructed using the Mag-TE technique (Ito et al., 2004a). First, MCLs (100-pg magnetite/cell) were added to CMs, in order to label cells magnetically. After a 4 h incubation period, CMs (1×10^6 cells/cm^2) were seeded onto the restricted area (15.5-mm diameter) that was surrounded by a silicone frame positioned at the center of a 100-mm ultra-low-attachment dish (Corning, NY). The surface of this dish was comprised of a covalently bound hydrogel layer that was hydrophilic and neutrally charged. A cylindrical neodymium magnet (diameter, 30 mm; height, 15 mm; magnetic induction, 4,000 Gauss) was then placed at the reverse side of the ultra-low-attachment dish to provide magnetic force vertical to the plate, and the cells were then cultured for 24 h.

Histological Examination

For histological evaluation, CMs sheets were washed with phosphate-buffered saline (PBS, pH 7.4) consisting of

DOI 10.1002/bit

137 mM NaCl (Wako, Osaka, Japan), 8.1 mM $Na_2HPO_4/12H_2O$ (Wako), 2.68 mM KCl (Wako), and 1.47 mM KH_2PO_4 (Wako), fixed in 10% formalin solution (Mildform®, Wako), and embedded in paraffin. Thin (4 μm) cross-sectional slices were stained by hematoxylin and eosin.

To examine the presence of gap junctions, CMs sheets constructed by Mag-TE were subjected to immunofluorescence staining with a connexin43-specific antibody. The CMs sheets were washed twice with PBS, fixed in 2.0% paraformaldehyde solution (Sigma-Aldrich), and embedded in Tissue-Tek OCT compound (Fisher Scientific, Bridgewater, NJ). Then, the embedded CM sheets were frozen and sectioned. The sections were incubated with a 1:200 dilution of rabbit anti-connexin43 (Zymed, San Francisco, CA) for 30 min and then were incubated with a 1:1,000 dilution of Alexa568-conjugated goat anti-rabbit IgG (Molecular probes, Eugene, OG) for 1 h. Samples processed without primary antibody or secondary antibody served as negative controls.

Measurement of Electrical Conduction

Electrical conduction within CM sheets constructed by Mag-TE was examined by extracellular potential mapping using a specifically designed multi-electrode array system (MED64, Panasonic, Tokyo, Japan). The microelectrodes (50 μm × 50 μm each) were arranged in an 8 × 8 pattern. The inter-electrode distance was 450 μm, and the electrodes covered a 3,150 μm × 3,150 μm area. To examine the electrical conduction of CMs within the sheets, CMs incubated in MCL-containing medium (100 pg/cell) for 4 h were seeded on multi-electrode arrays at the concentration of 1×10^6 cells/cm^2. Then, a magnet (4,000 G) was placed at the reverse side of the probe to allow cells to form a sheet-like structure. After 48 h of incubation, the electrical conduction was measured by multi-electrode extracellular potential mapping.

Results

MCL Uptake by CMs and Its Effect on CM Viability

To investigate the amount of MCL uptake by CMs, MCLs were added to the culture medium of CMs at concentrations of 25, 50, and 100 pg/cell (Fig. 1A). The uptake of magnetite nanoparticles increased to 27.5% of total added magnetite nanoparticles (uptake of 7.2, 13.2, and 27.3 pg/cell, for 25, 50, and 100 pg/cell, respectively) at 4 h after addition of MCLs and remained unchanged at the 24-h time point.

To examine the toxicity of MCLs, CMs were cultured without removal of MCLs (Fig. 1B). The number of viable cells at all MCLs concentrations was similar to those cell cultured without MCLs. Therefore, subsequent experiments utilized MCLs at a concentration of 100 pg/cell.

Construction of CM Sheets by Mag-TE

In order to construct the CM sheets, magnetically labeled CMs (1×10^6 cells/cm^2) were seeded into the restricted area (15.5-mm diameter) that was surrounded by a silicone frame positioned at the center of a 100-mm ultra-low-attachment dish. A magnet (4,000 G) was placed on the reverse side of the restricted area to allow accumulation of magnetically labeled cells in this area. After 24 h of incubation in the presence of a magnet, CMs accumulated to form a sheet-like structure (Fig. 2A). By contrast, CMs formed in a spheroid-shape when CMs were cultured

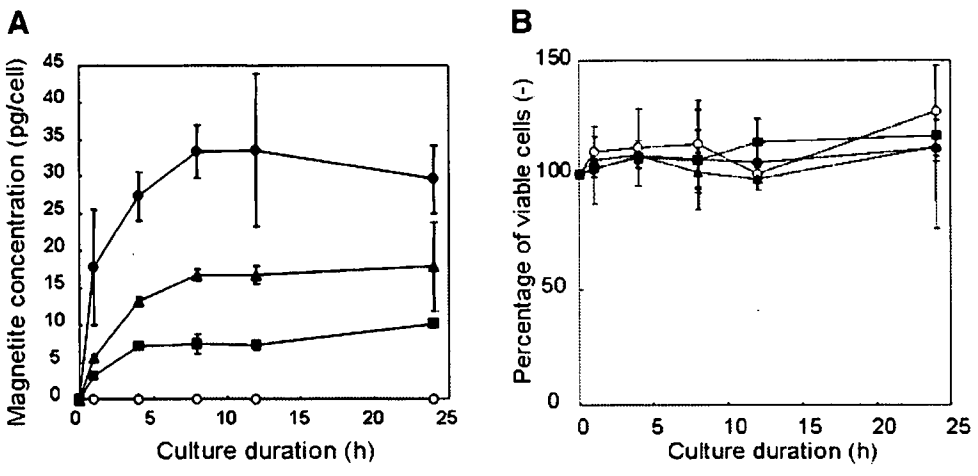

Figure 1. MCL uptake and percentage of viable CMs. **A**: Magnetite concentration in CMs after addition of MCLs was measured by the potassium thiocyanate method. **B**: Percentage of viable CMs after addition of MCLs was measured by the trypan blue dye-excluding method. Briefly, MCLs were added into the culture medium at the concentration of 0, 25, 50, and 100 pg/cell. After 0, 1, 4, 8, 12, and 24 h, the number of cells and the magnetite concentrations were measured. Addition of MCLs, 0 pg/cell (open circle); 25 pg/cell (closed square); 50 pg/cell (closed triangle); 100 pg/cell (closed circle). Data points represent the mean and SD of more than two independent studies.

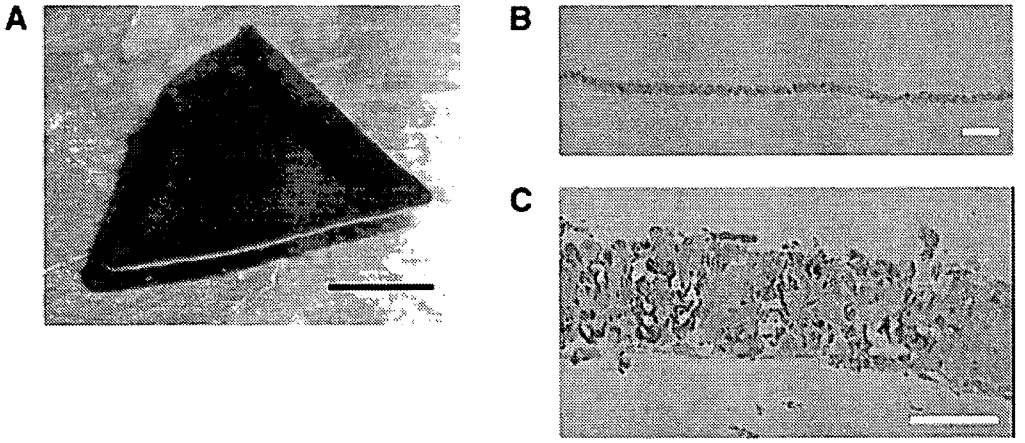

Figure 2. Bright-field photograph of CM sheet constructed by Mag-TE; scale bar, 5 mm (**A**). Bright-field photograph of hematoxylin and eosin (HE)-stained cross-sections of CM sheet; scale bar, 500 μm (**B**). Bight-field photograph with higher magnification of HE-stained cross-sections of CM sheet; scale bar, 100 μm (**C**). To label CMs magnetically, MCLs were added to the culture medium of CMs at the concentration of 100 pg/cell and incubated for 4 h. Then, the magnetically labeled CMs were recovered and used to construct the CM sheets. The CM sheets were fixed in 10% formalin solution and embedded in paraffin.

without a magnet on an ultra-low-attachment plate (data not shown). The CM sheets constructed by Mag-TE were black–brown in color, which was attributed to the magnetite nanoparticles. When the magnet was removed, the CM sheets detached from the surface of ultra-low-attachment dish and retracted slightly from the edge of the CM sheet (Fig. 2A). Hematoxylin and eosin staining within cross-section of CM sheets revealed that the CM sheets were contiguous and were approximately 120 μm in thickness (corresponding to about eight layers) (Fig. 2B and C). Immunofluorescent staining of connexin43 revealed the presence of gap junction within the CM sheets at 24 h after the seeding of CMs onto a magnet (Fig. 3A and B).

Electric Conduction of CMs in CM Sheets

Based on the presence of gap junctions within the CM sheet constructed by Mag-TE (Fig. 3A and B), the electrical conduction was also examined. The electrical conduction of CMs within CM sheets constructed by Mag-TE was measured by multi-electrode extracellular potential mapping. Figure 4A shows representative microelectrodes signals from the multi-electrode array system within a CM sheet. Electric signals were diffusely present and were recorded from more than half of the 64 electrodes. The position of the negative peak of the field potentials demonstrated that the electrical signal was generated in the vicinity of electrode no. 10 and that the conduction velocity across the CM sheet constructed by Mag-TE was 9.1 ± 1.8 cm/s, corresponding to the conduction velocity reported by Beeres et al. (2005). Figure 4B shows the frequency of beating in which the electrical spikes were synchronized at 22.6 beat per minute (bpm). These results suggest that electrical conduction was established between CMs within the CM sheets that were constructed by Mag-TE.

Discussion

The fabrication of 3-D constructs without artificial 3-D scaffolds is an ongoing challenge for tissue engineering.

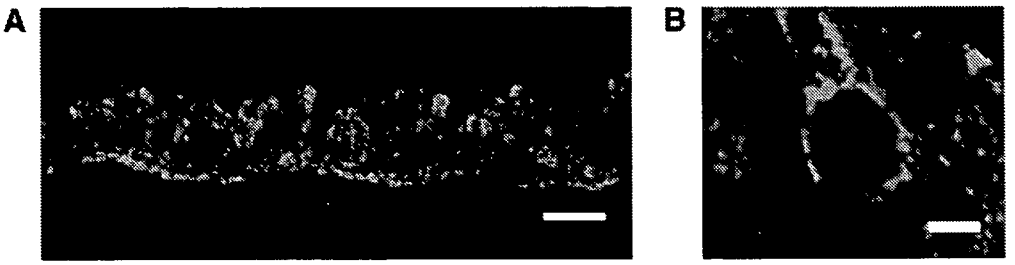

Figure 3. Cross-section appearance of immunological stained CM sheet with anti-connexin43 antibody; scale bar, 100 μm (**A**). Higher magnification; scale bar, 5 μm (**B**). The thin sections were incubated with a 1:200 dilution of rabbit anti-connexin43 (Zymed) for 30 min. Subsequently, the sections were incubated with a 1:1,000 dilution of Alexa568-conjugated goat anti-rabbit IgG (Molecular probes) for 1 h. Samples processed without primary antibody or secondary antibody served as negative controls.

DOI 10.1002/bit

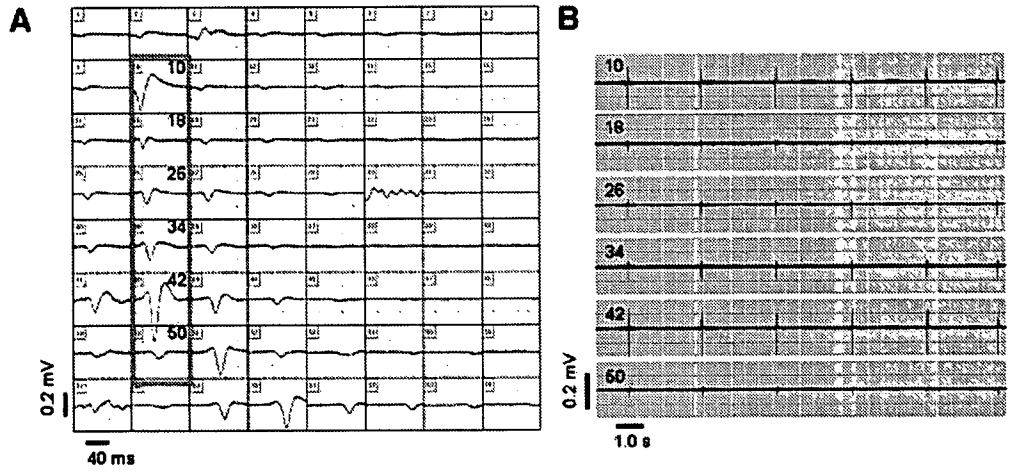

Figure 4. Representative signals from the multi-electrode extracellular potential mapping with 8 by 8 microelectrodes within the CM sheet constructed by Mag-TE, acquired (A). Signals recorded by six microelectrodes (marked numbers 10, 18, 26, 34, 42, and 50) in (A) (B). MCLs were added into the culture medium at the concentration of 100 pg/cell in order to label CMs magnetically. After 4 h incubation, the magnetically labeled CMs were seeded on multi-electrode array, and then a magnet (4,000 G) was placed at the reverse side of the probe to allow cells formed sheet-like structure. After 48 h of incubation, the electrical conduction was monitored.

Generally, in the first step of tissue engineering, target cells expanded in vitro are harvested from cell culture flask through the use of enzymes (e.g., trypsin or dispase) that digest the extracellular matrix (ECMs) and adhesive proteins. However, a lack of cell–cell adherence due to the enzymatic digestion makes reconstruction of 3-D tissue-like structure without scaffolds problematic.

Okano and colleagues developed a thermo-responsive culture surface grafted to poly (*N*-isopropylacrylamide) (PIPAAm) to form a "cell sheet" without scaffolds (Yamato and Okano, 2004). Cells that adhered to the thermo-responsive surface could proliferate on the PIPAAm dishes just as if they were cultured on polystyrene dishes. Furthermore, confluent cells on the PIPAAm dishes could be expelled as intact contiguous sheets by decreasing the temperature below the critical solution temperature of PIPAAm. Since this method did not utilize digestive enzymes to harvest cell sheets, the ECMs remained intact with enhanced cell–cell attachments. By contrast, Kelm and Fussenegger (2004) utilized a "microtissue" scaffold-free aggregation of cells (spheroid) technique to establish 3-D tissue-like structures. In this manner, cell reaggregation could be achieved using various methods, including cultivation on non-adhesive surfaces. When cells were seeded onto a tissue culture dish whose surface was non-adhesive, cells did not attach onto the culture surface, thereby resulting in spontaneous cell aggregations that were regarded as a 3-D microtissue.

Alternatively, our group developed a new methodology for tissue engineering, termed "Mag-TE" to fabricate scaffolds-free multi-layered cell sheets (Ito et al., 2004a, 2005a; Shimizu et al., 2006). In the present study, the contiguous CM sheets were constructed by Mag-TE (Fig. 2A–C). Although CMs formed spheroid when CMs were cultured without a magnet on an ultra-low-attachment plate (data not shown), CMs accumulated almost evenly onto the culture surface in the presence of a magnet (Fig. 2C). Indeed, the magnetic density detected at the surface of the magnet was approximately uniform throughout the cultured area (Ito et al., 2004a). These data indicate that CM sheets constructed by Mag-TE are a "magnetically shaped functional cell cluster," rather than a spontaneously shaped spheroid. Further investigation regarding the effect of magnetic force on sheet-like structure formation or the suitable amount of MCL uptake required for sheet-like structure formation would be of benefit.

Several studies of cell–cell adhesion and cell signaling within spheroids have provided evidence that 3-D anchorage-independent culture enhances expression of E-cadherin and other cell adhesion molecules (Kim et al., 2004; von Schlippe et al., 2000). Indeed, a previous study (Ito et al., 2004a) reported that desmosomes connect adjacent cells in keratinocyte sheets constructed by Mag-TE, suggesting that cadherins and other cell adhesion molecules are involved in sheet formation. In the present study, the presence of a major cardiac gap junction protein, connexin43 was certified by immunofluorescent staining (Fig. 3A). Moreover, electrical communications within CM sheets constructed by Mag-TE were confirmed by multi-electrode extracellular potential mapping (Fig. 4A and B). These results suggest that the cell–cell interactions were successfully established within CMs sheets constructed by Mag-TE. Indeed, this is the first report to demonstrate that the cell sheet constructed by Mag-TE was not just a "cell aggregate" formed by magnetic attraction, but rather a magnetically shaped "functional" cell cluster.

The conduction velocity of the CMs sheets constructed by Mag-TE was approximately 9.1 cm/s (Fig. 4A), which is consistent with previous reports (Beeres et al., 2005). Also, the beating rate of CMs sheets constructed by Mag-TE was approximately 23 bpm (Fig. 4B), which corresponds with the beating rate of CMs sheets that were constructed using a fibrin-coated cell culture dish (Itabashi et al., 2005). However, this rate is much slower than the beating rates of rat in the neonatal period (more than 300 bpm). Indeed, Itabashi et al. (2005) reported that the beating rate of CMs sheets was increased when the CMs sheets were cultured in static condition for 7 days. Therefore, the beating rate of CMs sheets constructed by Mag-TE may increase if the CMs sheets are cultured under appropriate condition. In the present study, the viability of CM sheets was not monitored for a long time. Since CM sheets contained a great number of cells, we suppose that heart tissue engineering-oriented bioreactors which can supply nutrients to each cell in the CM sheets constructed by Mag-TE are needed.

Toxicity of MCLs against CMs is an important consideration. MCLs are cationic liposomes containing 10-nm magnetite nanoparticles. Magnetite (Fe_3O_4) nanoparticles, as core elements of MCLs, have been clinically used as a contrast medium for magnetic resonance imaging (MRI). Also, the liposome consisting of three kinds of lipids, TMAG, DLPC, and DOPE (1:2:2 molar ratio) have been used as a safe liposomal vector for cancer gene therapy (Yoshida et al., 2004). Previous studies reported that MCLs did not inhibit the proliferation of several cell types within the magnetite concentration tested (human keratinocytes, <50 pg/cell (Ito et al., 2004a); human mesenchymal stem cells, <100 pg/cell (Ito et al., 2004b); human aortic endothelial cells, <100 pg/cell (Ito et al., 2004c); human aortic smooth muscle cells, <100 pg/cell (Ito et al., 2005c); normal human dermal fibroblast, <100 pg/cell (Ito et al., 2005c); human umbilical vascular endothelial cells, <100 pg/cell (Ito et al., 2005c)) and also revealed that human mesenchymal stem cells maintained an in vitro ability to differentiate into osteoblasts, adipocytes, or chondrocytes at a magnetite concentration below 100-pg magnetite/cell (Ito et al., 2004b, 2005b). In the present study, CM sheets were constructed at a magnetite concentration of 100 pg/cell. At this concentration, no decrease was observed in the percentage of viable CMs within 24 h of culture (Fig. 1B). Also, in preliminary experiments, propidium iodide (PI) staining failed to detect any increase in the number of dead cells at increasing concentrations of MCLs (data not shown). Moreover, there are possibilities that the magnetite nanoparticles inside the cells affect the electrical potential mapping of CM sheets. However, as described above, it was difficult to have control recordings from CM sheets without particles, because CMs formed in a spheroid-shape when CMs were cultured without a magnet or magnetite nanoparticles on an ultra-low-attachment plate (data not shown). However, when the CMs were cultured as monolayer, the effects of nanoparticles inside the CMs to the electrical potential mapping were monitored by multi-electrode extracellular potential mapping. Briefly, MCLs were added to the medium of CMs at the concentrations of 200 pg/cell, which was twice of the concentration used to construct CM sheets in the present study. After 4 h cultivation, the CMs labeled magnetically were collected and seeded onto the probe of multi-electrode extracellular potential mapping, and cultured for 48 h as monolayer. As a result, the conduction velocity of the CMs with MCLs was 11.9 + 2.9 cm/s, corresponding to the conduction velocity of CMs without MCLs reported previously (Inoue et al., 2004). Therefore, it was suggested that MCLs have no marked interference activities to the electrical potential mapping of CMs. However, further experiments are needed to evaluate the toxicity of MCLs against the electrical potential mapping in vivo.

In conclusion, the present study investigated the feasibility of a novel methodology called "Mag-TE" for the construction of CM sheets and demonstrated that the Mag-TE methodology was a potent tool for heart tissue engineering.

The work was partly supported by the grant from Ministry of Education, Sports, Science, and Technology, Japan, (17760622, 17066003, 18048024, 18038021) JSPS and 21st Century COE Program (Nature-Guided Materials Processing).

References

Akins RE, Boyce RA, Madonna ML, Schroedl NA, Gonda SR, McLaughlin TA, Hartzell CR. 1999. Cardiac organogenesis in vitro: Reestablishment of three-dimensional tissue architecture by dissociated neonatal rat ventricular cells. Tissue Eng 5:103–118.

Beeres SL, Atsma DE, van der Laarse A, Pijnappels DA, van Tuyn J, Fibbe WE, de Vries AA, Ypey DL, van der Wall EE, Schalij MJ. 2005. Human adult bone marrow mesenchymal stem cells repair experimental conduction block in rat cardiomyocyte cultures. J Am Coll Cardiol 46(10):1943–1952.

Carrier RL, Ppadaki M, Rupnick M, Schoen FJ, Bursac N, Langer R, Freed LE, Vunjak-Novakovic G. 1999. Cardiac tissue engineering: Cell seeding, cultivation parameters, and tissue construct characterization. Biotechnol Bioeng 64:580–589.

Inoue N, Ohkusa T, Nao T, Lee JK, Matsumoto T, Hisamatsu Y, Satoh T, Yano M, Yasui K, Kodama I, Matsuzaki M. 2004. Rapid electrical stimulation of contraction modulates gap junction protein in neonatal rat cultured cardiomyocytes. J Am Coll Cardiol 44:914–922.

Itabashi Y, Miyoshi S, Kawaguchi H, Yuasa S, Tanimoto K, Furuta A, Shimizu T, Okano T, Fukuda K, Ogawa S. 2005. A new method for manufacturing cardiac cell sheets using fibrin-coated dishes and its electrophysiological studies by optical mapping. Artif Organs 29(2):95–103.

Ito A, Hayashida M, Honda H, Hata K, Kagami H, Ueda M, Kobayashi T. 2004a. Construction and harvest of multilayered keratinocyte sheets using magnetite nanoparticles and magnetic force. Tissue Eng 10(5–6):873–880.

Ito A, Hibino E, Honda H, Hata K, Kagami H, Ueda M, Kobayashi T. 2004b. A new methodology of mesenchymal stem cell expansion using magnetic nanoparticles. Biochem Eng J 20:119–125.

Ito A, Takizawa Y, Honda H, Hata K, Kagami H, Ueda M, Kobayashi T. 2004c. Tissue engineering using magnetite nanoparticles and magnetic force: Heterotypic layers of cocultured hepatocytes and endothelial cells. Tissue Eng 10(5–6):833–840.

DOI 10.1002/bit

Ito A, Hibino E, Kobayashi C, Terasaki H, Kagami H, Ueda M, Kobayashi T, Honda H. 2005a. Construction and delivery of tissue-engineered human retinal pigment epithelial cell sheets, using magnetite nanoparticles and magnetic force. Tissue Eng 11(3–4):489–496.

Ito A, Hibino E, Shimizu K, Kobayashi T, Yamada Y, Hibi H, Ueda M, Honda H. 2005b. Magnetic force-based mesenchymal stem cell expansion using antibody-conjugated magnetoliposomes. J Biomed Mater Res B Appl Biomater 75(2):320–327.

Ito A, Ino K, Hayashida M, Kobayashi T, Matsunuma H, Kagami H, Ueda M, Honda H. 2005c. Novel methodology for fabrication of tissue-engineered tubular constructs using magnetite nanoparticles and magnetic force. Tissue Eng 11(9–10):1553–1561.

Kelm JM, Fussenegger M. 2004. Microscale tissue engineering using gravity-enforced cell assembly. Trends Biotechnol 22(4):195–202.

Kim JB, Stein R, O'Hare MJ. 2004. Three-dimensional in vitro tissue culture models of breast cancer—A review. Breast Cancer Res Treat 85(3):281–291.

Langer R, Vacanti JP. 1993. Tissue engineering. Science 260(5110):920–926.

Miltenyi S, Muller W, Weichel W, Radbruch A. 1990. High gradient magnetic cell separation with MACS. Cytometry 11(2):231–238.

Moore LR, Zborowski M, Sun L, Chalmers JJ. 1998. Lymphocyte fractionation using immunomagnetic colloid and a dipole magnet flow cell sorter. J Biochem Biophys Methods 37(1–2):11–33.

Owen CS, Sykes NL. 1984. Magnetic labeling and cell sorting. J Immunol Methods 73(1):41–48.

Papadaki M, Bursac N, Langer R, Merok J, Vunjak-Novakovic G, Freed LE. 2001. Tissue engineering of functional cardiac muscle: Molecular, structural, and electrophysiological studies. Am J Physiol Heart Circ Physiol 280:H168–H178.

Radbruch A, Mechtold B, Thiel A, Miltenyi S, Pfluger E. 1994. High-gradient magnetic cell sorting. Methods Cell Biol 42(Pt B):387–403.

Shimizu K, Ito A, Honda H. 2005. Enhanced cell-seeding into 3D porous scaffolds by use of magnetite nanoparticles. J Biomed Mater Res B Appl Biomater 77:265–272.

Shimizu K, Ito A, Yoshida T, Yamada Y, Ueda M, Honda H. 2006. Bone tissue engineering with human mesenchymal stem cell sheets constructed using magnetite nanoparticles and magnetic force. J Biomed Mater Res B Appl Biomater. in press.

Shinkai M, Yanase M, Honda H, Wakabayashi T, Yoshida J, Kobayashi T. 1996. Intracellular hyperthermia for cancer using magnetite cationic liposomes: In vitro study. Jpn J Cancer Res 87:1179–1183.

von Schlippe M, Marshall JF, Perry P, Stone M, Zhu AJ, Hart IR. 2000. Functional interaction between E-cadherin and alphav-containing integrins in carcinoma cells. J Cell Sci 113(Pt 3):425–437.

Yamato M, Okano T. 2004. Cell sheet engineering. Mater Today 7:42–47.

Yoshida J, Mizuno M, Wakabayashi T. 2004. Interferon-beta gene therapy for cancer: Basic research to clinical application. Cancer Sci 95(11):858–865.

Zammaretti P, Jaconi M. 2004. Cardiac tissue engineering: Regeneration of the wounded heart. Curr Opin Biotechnol 15(5):430–434.

Zimmermann WH, Melnychenko I, Eschenhagen T. 2004. Engineered heart tissue for regeneration of diseased hearts. Biomaterials 25(9):1639–1647.

THE JOURNAL OF BIOLOGICAL CHEMISTRY VOL. 281, NO. 4, pp. 2390–2400, January 27, 2006

Versican/PG-M Regulates Chondrogenesis as an Extracellular Matrix Molecule Crucial for Mesenchymal Condensation*

Received for publication, August 24, 2005, and in revised form, October 24, 2005 Published, JBC Papers in Press, October 28, 2005, DOI 10.1074/jbc.M509341200

Nobuhiro Kamiya[‡§1], Hideto Watanabe[‡], Hiroko Habuchi[‡], Hidekazu Takagi[‡], Tamayuki Shinomura[‡2], Katsuji Shimizu[§], and Koji Kimata[‡3]

From the [‡]Institute for Molecular Science of Medicine, Aichi Medical University, Nagakute, Aichi 480-1195 and the [§]Department of Orthopaedic Surgery, Gifu University, Gifu 500-8705, Japan

Mesenchymal cell condensation is an essential step for cartilage development. Versican/PG-M, a large chondroitin sulfate proteoglycan, is one of the major molecules expressed in the extracellular matrix during condensation. However, its role, especially as an environment for cells being condensed, has not been elucidated. Here we showed several lines of evidence for essential roles of versican/PG-M in chondrogenic condensation using a new chondrocytic cell line, N1511. Chondrogenic stimuli (treatment with parathyroid hormone, dexamethasone, 10% serum) induced a marked increase in the transcription and protein synthesis of versican/PG-M. Stable antisense clones for versican/PG-M, depending on suppression of the expression of versican/PG-M, showed different capacities for chondrogenesis, as indicated by the expression and deposition of aggrecan, a major chondrocytic cell product. The cells in the early stages of the culture only expressed V0 and V1 forms, having more chondroitin sulfate chains among the four variants of versican/PG-M, and treatment of those cells with chondroitinase ABC suppressed subsequent chondrogenesis. Furthermore, treatment with β-xyloside, an artificial chain initiator of chondroitin sulfate synthesis to consequently inhibit the synthesis on the core proteins, suppressed chondrogenesis. In addition, forced expression of the variant V3, which has no chondroitin sulfate chain, disrupted the deposition and organization of native versican/PG-M (V0/V1) and other extracellular matrix molecules known to be expressed during the mesenchymal condensation and resulted in the inhibition of subsequent chondrogenesis. These results suggest that versican/PG-M is involved in positively regulating the formation of the mesenchymal matrix and the onset of chondrocyte differentiation through the attached chondroitin sulfate chains.

Mesenchymal cell condensation is the first step of organogenesis in many tissues. Cartilage formation in limb buds, one of the most typical examples of organogenesis, starts with the condensation of chondrogenic mesenchymal cells (1). This step is thought to be essential for subsequent skeletal development in vertebrates (2) and requires the involvement of not only some cell growth and morphogenetic factors, such as transforming growth factor-β (3), growth differentiation factor-5 (4), and bone morphogenetic proteins (BMPs)[4] (5), but also some cellular adhesion and extracellular matrix molecules such as N-cadherin (6), neural cell adhesion molecule (7), fibronectin (8), tenascin (9), versican/PG-M (10), hyaluronan (11), syndecan (12), and perlecan (13).

Versican/PG-M was originally isolated as PG-M (medium-sized chondroitin sulfate proteoglycan) from the core (the mesenchymal cell condensation area) of chick embryonic limb bud at stage 23 (10). The cDNA of versican/PG-M was cloned as versican, a fibroblast proteoglycan (14), and also as one of the alternatively spliced forms of the PG-M core protein (15). Versican/PG-M has a molecular mass of more than 1,000 kDa and consists of two globular domains at the N and C termini (G1 and G3 domain, respectively) and the two chondroitin sulfate-attachment domains (CS-α and CS-β) (16, also see Fig. 4*A*). The G1 and G3 domains are commonly found in proteoglycans belonging to the aggrecan family and are binding sites for hyaluronan and oligosaccharides, respectively (17, 18). The CS-α and CS-β domains give unique properties to this proteoglycan in that multiple alternative splicing yields the following four variant forms with different numbers of the attached chondroitin sulfate chains: V0 having CS-α and CS-β, V1 having CS-β, V2 having CS-α, and V3 having neither of the two (19 in chicken; 15, 16, and 20 in mouse; 14 and 21 in human). An important role for versican/PG-M in the condensation process has been suggested by its unique properties as follows: 1) high transient expression in the mesenchymal cell condensation area during development of cartilage (10, 22–24), heart (25, 26), hair follicles (25), and kidney (27); 2) specific binding to fibronectin (28), type I collagen (28), hyaluronan (11, 29), and tenascin (9), also major matrix molecules in the mesenchymal cell condensation area; and 3) ability to inhibit cell adhesion to a variety of extracellular matrix molecules such as fibronectin or type I collagen through its chondroitin sulfate chains (30–32). Versican/PG-M interacts with cell surface annexin VI and inhibits the subsequent cell-spreading step that needs the rearrangement of cytoskeletal elements (33).

Exogenous treatment with versican/PG-M of mesenchymal cells isolated from chick embryonic limb buds at stage 22/23 inhibited their spreading onto the substrates and enhanced their aggregation and further differentiation into chondrocytes (34). Previous studies reported that chondrocyte shape influences the differentiation via changes in

* This work was supported in part by grants-in-aid for scientific research (B) from the Japan Society for the Promotion of Science, by a Grant-in-aid for Scientific Research on Priority Areas 14082206 from the Ministry of Education, Culture, Sports, Science and Technology of Japan, and by a special research fund from Seikagaku Corp. The costs of publication of this article were defrayed in part by the payment of page charges. This article must therefore be hereby marked "*advertisement*" in accordance with 18 U.S.C. Section 1734 solely to indicate this fact.

[1] Present address: Laboratory of Reproductive and Developmental Toxicology, NIEHS, National Institutes of Health, Research Triangle Park, NC 27709.

[2] Present address: Dept. of Hard Tissue Engineering, Tokyo Medical and Dental University, Tokyo 113-8549, Japan.

[3] To whom correspondence should be addressed: Institute for Molecular Science of Medicine, Aichi Medical University, Nagakute, Aichi, 480-1195, Japan. Tel.: 81-561-62-3311 (ext. 2088); Fax: 81-561-63-3532; E-mail: kimata@aichi-med-u.ac.jp.

[4] The abbreviations used are: BMPs, bone morphogenetic proteins; ECM, extracellular matrix; FCS, fetal calf serum; PTH, parathyroid hormone; CS, chondroitin sulfate; AS, antisense; HA, hyaluronan; FN, fibronectin; RT, reverse transcription; G1, globular domain number 1; G3, globular domain number 3; CS-α, the chondroitin sulfate-attached domain-a; CS-β, the chondroitin sulfate-attached domain-b; DAB, 3,3′-diaminobenzidine-HCl; GAPDH, glyceraldehyde-3-phosphate dehydrogenase; α-MEM, minimum essential medium α; FITC, fluorescein isothiocyanate; AS, antisense; P/D, PTH and dexamethasone; PBS, phosphate-buffered saline; PTHrP, parathyroid hormone-related protein.

cytoskeletal elements (35), and it can be regulated by interactions between matrix substrate molecules and receptors on the cell surface under the optimum condition of high cell density. Versican/PG-M also modulates embryonic chondrocyte morphology (36). We hypothesize that versican/PG-M is greatly involved in the mesenchymal cell condensation and subsequent chondrogenesis by modifying cell-extracellular matrix molecule interactions so as to influence the cell shape. To address this hypothesis, null mutation of the versican/PG-M gene in murine was supposed to provide direct results. However, this mutation resulted in embryonic death at 10.5 days post-coitum because of a heart abnormality before the onset of the chondrogenic mensenchymal cell condensation (37), and so no direct evidence has been obtained for the above hypothesis.

The transfection of mesenchymal cells in culture with sense or antisense cDNA in expression vectors might also have provided some evidence. However, primary cell cultures are not ideal systems to pursue such experiments because of the limited number of mesenchymal cells at the same stage as well as the instability of their phenotype. We have recently established a chondrocytic cell line, N1511 without transformation (38). In N1511 cells, the entire process of chondrogenic differentiation, including mesenchymal cell condensation, can be reproduced by treatment with natural growth factors and cytokines, as characterized by changes in cell morphology and the onset of the expression of cartilage-specific genes such as type I, II, IX, and X collagen and aggrecan. These properties reflect well the *in vivo* chondrogenesis and further chondrocyte differentiation, suggesting that N1511 cells could provide an *in vitro* model system to study cartilage development from the step of a mensenchymal condensation as a process of groundwork for further differentiation.

In this study, we first demonstrate that, immediately after induction, N1511 cells expressed versican/PG-M (V0 and V1 forms) at a high level, resembling the *in vivo* phenotype of condensing mesenchymal cells in the early phase, and then differentiated into chondrocytes. We next examined the effect of abrogation of versican/PG-M expression and interruption of versican/PG-M deposition into the matrix during the multiple steps of the chondrogenesis of N1511 cells. The inhibition by antisense of the synthesis of versican/PG-M suppressed chondrogenesis assessed by the gene expression and deposition in the matrix of aggrecan. In addition, overexpressed V3, which is the smallest spliced variant form of versican/PG-M without both chondroitin sulfate attachment domains, affected the deposition of native (endogenously produced) versican/PG-M in the ECM and also resulted in the suppression of chondrogenic differentiation. Furthermore, reduction of chondroitin sulfate chains in the ECM by chondroitinase ABC digestion and inhibition of native synthesis of chondroitin sulfate chains on the core proteins by β-xyloside treatment suppressed chondrogenesis. These results indicate that V0 and V1 forms of versican/PG-M expressed in the early phase of chondrogenesis serve as ECM molecules involved in mesenchymal cell condensation and promote further chondrocyte differentiation. Evidence is also provided that chondroitin sulfate chains of those proteoglycans are functional sites for the modification of cell-matrix interactions during mesenchymal condensation and the subsequent steps of chondrogenesis.

EXPERIMENTAL PROCEDURES

Cell Line and Culture Conditions—N1511 cells, a cell line established from chondrocytic cells in the rib cage of a 4-week-old male p53-null mouse, reproduce each step of chondrogenesis (38). The cells were maintained in minimum essential medium α (α-MEM) supplemented with 10% fetal calf serum (FCS), penicillin, and streptomycin at 37 °C in 5% CO_2 until 80% confluent. The cells were then plated at a density of 1.5×10^6 cells/35-mm dish, and after 24 h (defined as day 0), chondrogenesis was induced by combined treatment with 1×10^{-6} M dexamethasone (Calbiochem) and 1×10^{-7} M rat PTH-(1–34) (Sigma) in the presence of 10% FCS. The medium was changed every other day.

Transfection—The cells at 40% confluency in 100-mm dishes were cotransfected with 3 μg of vector containing antisense strand, vector containing sense strand, or vector alone (mock) and 0.1 μg of PurR plasmid vector, using 12 μl of TransIT-LT1 reagent (Mirus Corp., Madison, WI) and 500 μl of Opti-MEM™ (Invitrogen) in 10 ml of α-MEM containing 10% FCS. The transfectants were screened with 5 μg/ml puromycin for 3 days, and a pool of stable transfectants was again screened for 2 days using 5 μg/ml puromycin. We also transfected the cells with vector containing the smallest spliced form (V3) of versican/PG-M to examine the effect of a transient overexpression. To improve the transfection efficiency and to remove the effect of the untransfected cell debris on the cell adhesion, the transfection was performed at 40% confluency in 100-mm dishes. After 24 h of transfection, the cells were trypsinized and re-plated in the 35-mm dishes at a density of 1.5×10^6 cells/dish.

Antibodies, Immunofluorescent Staining, and Alcian Blue Staining—For rabbit antibodies against the alternatively spliced domain, CS-β, the cDNA fragment encoding this region was inserted into the protein A gene fusion vector, pRIT-2T (Amersham Biosciences). The fusion protein produced in transfected *Escherichia coli* N4830-1 was purified from cell lysate using IgG-Sepharose 6 Fast Flow and used for immunization. The antibodies obtained were designated anti-mouse CS-β domain antibodies. Rabbit polyclonal antibodies against rat aggrecan also proven to be specific for mouse aggrecan (38) were a gift from Dr. Yada in this laboratory. 2B1, a mouse monoclonal antibody against versican/PG-M purified from human yolk sac tumor (39), and biotinylated HA-binding protein (40) were purchased from Seikagaku Corp. (Tokyo, Japan). A polyclonal antibody against mouse fibronectin was obtained from Santa Cruz Biotechnology (Santa Cruz, CA). For immunostaining, whole-mount cultures at appropriate time points were rinsed with PBS, fixed with 10% formalin/PBS for 10 min at room temperature, and then incubated for 1 h with the following primary antibodies at the indicated dilution, respectively: anti-mouse CS-β domain antibodies (dilution, 1:1000), anti-mouse aggrecan antibodies (1:100), monoclonal antibody for human versican/PG-M, 2B1 (1:100), and anti-fibronectin antibody (1:100). For the fluorescent staining, Alexa Fluor™ 488 and 596 of goat anti-rabbit IgG antibodies and goat anti-mouse IgG antibodies, respectively (Molecular Probes, Eugene, OR), were used for 1 h as secondary antibodies (1:1000). For the immunochemical staining, Histofine kits using biotinylated anti-rabbit or anti-mouse IgG antibodies as secondary antibodies and peroxidase-conjugated streptavidin and 3,3′-diaminobenzidine-HCl (DAB) as color-developing reagents (Nitirei, Tokyo, Japan) were used. Biotinylated HA-binding protein (1:500) (Seikagaku Corp., Tokyo, Japan) and FITC-conjugated streptavidin (1:1000; Molecular Probes, Eugene, OR) were used for HA staining as described previously (40). For Alcian blue staining, the cultures were stained with 0.5% Alcian blue 8GX (Sigma) in 0.1 M HCl, pH 2.0, overnight and destained with 0.1 M HCl for 10 min as described previously (38). Photographs of stained cultures were taken using a CCD camera under the same conditions. Immunostained and Alcian blue-positive areas (at least 50 areas that were obtained by three independent experiments performed in triplicate) were quantitatively measured with NIH IMAGE software (version 1.57).

Treatment with Chondroitinase ABC—Five units/ml protease-free chondroitinase ABC (Seikagaku Corp., Tokyo, Japan) was treated in the

culture medium (2 ml of media/35-mm dish) up to day 4 every other day, and the cells were then rinsed with PBS several times and cultured in the regular induction medium for a further 2 weeks. For the digestion of the chondroitin sulfate chains, protein samples in the extracts with RIPA buffer containing protease inhibitors (50 mM Tris-HCl, pH 7.4, 150 mM NaCl, 1% Nonidet P-40, 0.25% sodium deoxycholate, 1 mM EDTA, 2 mM phenylmethylsulfonyl fluoride, and 3.6 mM pepstatin A) were treated with 5 units of chondroitinase ABC in the presence of protease inhibitors (41) at 37 °C for 45 min. After being boiled for 2 min at 100 °C, samples containing 50 mg of proteins were subjected to SDS-PAGE with a stacking gel of 3.75% (w/v) and a separation gel of 5% (w/v) acrylamide and transferred to polyvinylidene difluoride membranes as described previously (23). The core protein derivatives of versican/PG-M were detected immunochemically by using the anti-mouse CS-β domain antibodies and peroxidase-conjugated goat anti-rabbit IgG, and blots were visualized using the ECL chemiluminescence detection system (Amersham Biosciences).

Treatment with β-Xyloside—β-Xyloside, xyloside-*S*-$(CH_2)_6$-CH_3 (42), was dissolved in ethanol and stored at −20 °C (0.2 M). The cultures (35-mm dish) were treated with up to 2.0 mM of β-xyloside from day 0 to day 5, rinsed with PBS several times, and cultured in the regular induction medium for a further 2 weeks. The cell layer and medium were harvested at the indicated days. α-Xyloside was used for a negative control. The cultured medium was combined from day 1 to day 5 and precipitated with 3 volumes of cold ethanol containing 1.3% potassium acetate. These precipitates and cell layers were suspended in 2 or 1 ml of 0.2 M NaOH, respectively, incubated for 16 h at room temperature, neutralized with 4 M acetic acid added to a final concentration of 10 mM $MgCl_2$, and then treated with DNase (100 μg) and RNase (100 μg) at 37 °C for 2 h. Proteinase K (100 μg) was added, and incubation was continued for 16 h at 37 °C. The samples were centrifuged at 13,000 rpm for 10 min to remove insoluble materials. The supernatants were diluted with 1 volume of 20 mM Tris-HCl buffer, pH 7.2, and applied to a DEAE-Sephacel column equilibrated with 50 mM Tris-HCl buffer, pH 7.2, containing 0.2 M NaCl and subsequently washed with 10 column volumes of 0.2 M NaCl in 50 mM Tris-HCl buffer, pH 7.2. The fractions eluted with 2.0 M NaCl in the same buffer were collected. Three volumes of cold ethanol containing 1.3% potassium acetate were added to these fractions, and the glycosaminoglycans were recovered as precipitates by centrifugation at 13,000 rpm for 30 min at 4 °C. The precipitates were dissolved in water, and portions of the solutions were digested with chondroitinase ABC as described previously (43). The digests were analyzed by a reversed phase ion-pair chromatography using Senshu Pak column. The amounts of CS were estimated from their absorbance on the chromatographic patterns using standard disaccharides as described previously (43).

Constructions of Vectors for Antisense Inhibition and for Expression of V3—The versican/PG-M antisense vector was constructed using the −99 to +359 portion of the cDNA region as described previously (32). The fragment containing this region was amplified by PCR using primers (sense, 5′-GCTTCCTATGTGATCTTCCG-3′, and antisense, 5′-AGTTTGACCATGGTGAGGGA-3′), purified by agarose gel electrophoresis, and ligated into a SmaI site of the expression vector pKCR with the SV40 promoter. To confirm the direction of the inserted fragment, the plasmid was digested with PstI and sequenced.

A plasmid containing full-length mouse V3 cDNA was a gift from Dr. Zako in this laboratory (20). The cDNA fragment was excised with HindIII and EcoRI and subcloned into pSP72 cloning vector (Promega, Madison, WI). PCR was performed with 5′-GTGCGCCACCCTGTGACTGTG-3′ and 5′-ATCTTGCTCACAGAGTGCACCAAC-3′ as primers and human V3 cDNA (44) as a template. The PCR fragment (340 bp) was digested with DraIII and ligated into pSP72, which was digested with DraIII and subsequently with HindIII and EcoRI, and the fragment was subcloned into an expression vector pKCR. This plasmid, designated mhV3/pKCR, expresses mouse V3 with a human-specific epitope of 2B1. The epitope of 2B1 was in the human G3 domain.[5]

Northern Blotting, Quantitative Real Time PCR, and RT-PCR—Total RNA was prepared by using an RNeasy™ total RNA system (Qiagen Inc., Santa Clarita, CA). Twenty micrograms of total RNA was separated on a 1% agarose gel and transferred to a Duralon-UV membrane (Stratagene, La Jolla, CA). Filters were hybridized with mouse versican/PG-M or rat aggrecan probe. Mouse versican/PG-M probe and rat aggrecan cDNA were gifts from Dr. Zako and Dr. Yada in this laboratory, respectively. Each probe was ^{32}P-radiolabeled using a Random Primed DNA labeling kit (Roche Applied Science). To normalize mRNA levels, 28 S ribosomal RNA was used.

At various time points, mRNA was isolated from N1511 cells using a Micro-FastTrack™ 2.0 kit (Invitrogen), and cDNA was synthesized with the SuperScript™ preamplification system (Invitrogen). The mouse versican/PG-M primers, mouse aggrecan primers, and their TaqMan probes were designed using Primer Express software (Applied Biosystems, Foster City, CA). The TaqMan probe contained a reporter dye at the 5′ end and a quencher dye at the 3′ end. The sequences of the primers and the probes for mouse versican/PG-M are as follows: forward primer, 5′-CCAGTGTGAACTTGATTTTGATGAA-3′, and reverse primer, 5′-AACATAACTTGGGAGACAGAGACATCT-3′; TaqMan probe, 5′-CACTCTAACCCTTGTCGGAATGGT-3′. Those for mouse aggrecan are as described previously (45). These sequences are based on data in GenBank™, and the accession numbers for mouse versican/PG-M and mouse aggrecan are D28599 and U22901, respectively. As this primer-probe set was designed using the G3 domain of versican/PG-M, it can detect all the variants except mhV3. The RT-PCR was carried out with an ABI PRISM 7700. The reaction mixture (50 μl) contained 40 ng of total RNA, 200 μM of the primers, and 600 μM of probe in 1× TaqMan Universal PCR Master Mix (Rosh, Branchburg, NJ). TaqMan rodent GAPDH control reagents were used as the internal controls. The reverse transcription reaction was run, according to the manufacturer's recommended program. Data quantification and analysis were also performed according to the manufacturer's directions (PE Biosystems). Amplified fragments (108 and 80 bp, versican/PG-M and aggrecan) were sequenced for confirmation. Values represent levels relative to the control. Three independent experiments were performed in triplicate to obtain the values.

For detection of splicing variants of versican/PG-M, PCR amplification was performed using ExTaq™ (Takara Biomedicals, Kyoto, Japan) for 25 cycles under the following conditions: 94 °C for 15 s, 60 °C for 30 s, and 72 °C for 30 s. Forward primer 1, 5′-AGGTCAGAGAAAACAAGACAG-3′ (nucleotide 4080–4100 of mouse versican/PG-M cDNA), and forward primer 2, 5′-GCAGATTTGATGCCTACTGC-3′ (1194 to 1123), were used for V0 and V1–V3, respectively. Reverse primer 1, 5′-ACGGAGTAGTTGTTACATCCG-3′ (4316 to 4296), reverse primer 2, 5′-CTAATCTGCCTGTGATAGCC-3′ (1448 to 1429), and reverse primer 3, 5′-CTTGTTCACAGAGTGCACC-3′ (9557 to 9539), were used for V0/V1, V2, and V3, respectively (46). These amplified fragments were electrophoresed in 2% agarose gel (NuSieve). PCR products were sequenced. To standardize mRNA levels, the primers for mouse GAPDH were used as an internal control.

[5] M. Imagawa, T. Shinomura, and K. Kimata, unpublished observations.